AD-A159 359 ACTIVE IONOSPHERIC GENERATION OF ELF/VLF WAVES(U) 1/2
SCIENCE APPLICATIONS INTERNATIONAL CORP MCLEAN VA
K PAPADOPOULOS ET AL. 15 AUG 85 SAIC-85/1080
UNCLASSIFIED N00014-84-C-0353 F/G 4/1 NL

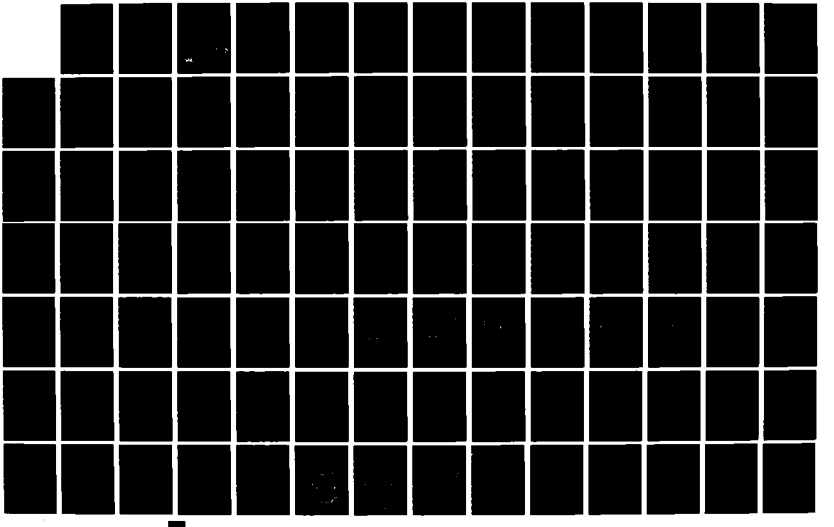

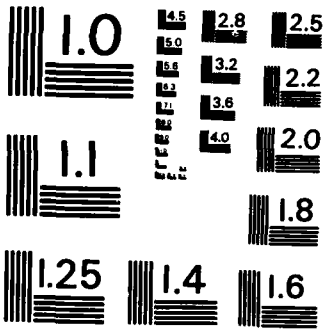

(2)

# ACTIVE IONOSPHERIC GENERATION OF ELF/VLF WAVES

K. PAPADOPOULOS, C.L. CHANG, K. KO,
AND Ç. MENYUK

FINAL REPORT NO. SAIC 85/1800

AUGUST 15, 1985









Science Applications International Corporation

# ACTIVE IONOSPHERIC GENERATION OF ELF/VLF WAVES

K. PAPADOPOULOS, C.L. CHANG, K. KO,
AND C. MENYUK

FINAL REPORT NO. SAIC 85/1800

AUGUST 15, 1985





SAIC™
Science Applications International Corporation
Post Office Box 1303, 1710 Goodridge Drive, McLean, Virginia 22102, (703) 821-4300

# ACTIVE IONOSPHERIC GENERATION OF ELF/VLF WAVES

K. Papadopoulos, C.L. Chang, K. Ko, and C. Menyuk

Final Report No. SAIC 85/1800

Submitted to

Office of Naval Research
Electronics Division
Pasadena, California 91106

In partial fulfillment of

Contract N00014-84-C-0353

August 15, 1985

## SUMMARY

During the past year our work supported by the ONR Contract N00014-84-C-0353 achieved many significant results concerning ionospheric generation of ELF/VLF as well as ULF waves. A major breakthrough was our participation in an experiment using the Arecibo facility in which a preliminary proof of principle of two of the relevant concepts was produced. We highlight below some of our key results and refer the interested reader to the appendices for details.

(i) A novel process for generating ELF/ULF waves by using ionospheric heating was discovered and its applicability to auroral geometry was exmined. The process relies on modulated E-region heating and does not depend on the preence of ambient ionospheric currents. The ELF/ULF signals are caused by oscillatory ionospheric currents spontaneously generated in the HF heated volume by the coupling of the hot spot temperature gradient ($\nabla T$) to the ambient ionospheric density gradient ($\nabla n \times \nabla T$). The mechanism can account for the remarkably large ULF signals observed by the Tromso HF modifications facility. The details can be found in a paper published in Geophysical Research Letters, 12, 279, (1985) and included as Appendix I.

(ii) A comprehensive analytic and computational study of the ELF generation by stimulated beat excitation in a dissipative medium was completed. The power thresholds that lead to complete pump decay for a transmitter with 30° incidence at various ionospheric heights are given in Table I of Appendix II along with the required pump frequency and the resulting low frequency. The details can be found in a paper accepted for publication in the Journal of Geophysical Research and included here as Appendix II.

(iii) We participated in the experimental program of Dr. Ganguly (Rice University) using the Arecibo facility. The experiment produced signals at 3 and 5 Hz of the order of 1 $m\gamma$ when operated under conditions appropriate for stimulated beat excitation. ULF waves with comparable amplitude were also produced by using the technique mentioned in (i) above. The interaction occurred in the F-region and therefore it was different than the current modulation schemes. The work will be presented as an invited paper at the APS Plasma Physics Meeting in San Diego, November 1985. The details can be found in a paper submitted to Phys. Rev. Lett. and included as Appendix III.

(iv) The structure and properties of the ELF plasma eigenmodes in the polar E-region of the ionosphere was examined in detail. It was noted that for altitudes below 150km the ion neutral collision frequency ($\nu_i$) is larger

than the ion cyclotron frequency ($\Omega_i$) thereby preventing the existence of proper Alfven or magnetosonic eigenmodes. Our work, however, indicates that the strong ion collisionality ($\nu_i > \Omega_i$) freezes the ion motion. This result shows that the whistler mode becomes a helicon right hand polarized mode for frequencies $\omega_{LF} < \nu_i$. This is similar in nature to the well known in solid state physics helicon mode, in which case the lattice rather than the collisionality freezes the ion motion. Since both the downconversion efficiency and the coupling of the ELF signals to the earth ionosphere waveguide favor low altitudes, it was concluded that the nonlinear coupling should be to the helicon rather than the Alfven or magnetosonic mode. A draft of the paper, is included as Appendix IV.

(v) Our most recent work, left unfinished due to the termination of the contract, focused on the possibility of generating oscillatory magnetic moments that radiate at ELF/VLF frequencies in the ionosphere by utilizing resonance absorption generated magnetic fields. The field generation by this process has been studied both theoretically (Bezzerides et al., Phys. Rev. Lett. 38, 663, 1977) and experimentally (DiVergilio et al., Phys. Rev. Lett. 38, 541, 1977; Obenschain and Luhmann, Jr., Phys. Rev. Lett. 42, 311, 1979) for the case of laser or microwaves interacting with the plasma. The saturated value of the self generated field

by radiowaves with frequency $f = \omega_o/2\pi$ and quiver velocity $V = eE/m\omega_o$ is (Bezzerides et al., Phys. Rev. Lett. 38, 495, 1977)

$$B = \frac{2mc}{e} \frac{\omega_e^2}{\omega_o c^2} \frac{e^2E^2}{m^2\omega_o^2} \qquad (1)$$

where $\omega_e$ is the plasma frequency.

In practical units this gives

$$B = 3.5\times10^{-1} \left[ \frac{n_o}{10^4 cm^{-3}} \right] \left[ \frac{MHz}{f_o} \right]^3 \left[ \frac{km}{L_T} \right]^2 \left[ \frac{P}{MW} \right] \gamma \quad (2)$$

where $L_T$ is the size of the hot spot in the resonance region as determined by the antenna gain, and P the RF power. This produces a magnetic moment M(t) of

$$M(t) = BL_N L_T^2 = 1.8 \times 10^8 \left[ \frac{n_o}{10^4 cm^{-3}} \right] \left[ \frac{MHz}{f_o} \right]^3 \times$$

$$\times \left[ \frac{L_N}{5km} \right] \left[ \frac{P}{10MW} \right] A\text{-}m^2 \qquad (3)$$

corresponding to a power $P_{VLF}$ at the modulating frequency f of

$$P_{VLF} = 5.3 \left[ \frac{f}{20kHz} \right]^4 \left[ \frac{n_o}{10^4 cm^{-3}} \right] \left[ \frac{MH_z}{f_o} \right]^3 \left[ \frac{L_N}{5km} \right] x$$

$$x \left[ \frac{P}{10MW} \right] kW. \qquad (4)$$

The magnetic field $\tilde{B}$ on the ground at a radius distance r from the modulated region will be

$$\tilde{B} = 2.6x10^{-1} \left[ \frac{100km}{h} \right]^{1/2} \left[ \frac{100km}{r} \right]^{1/2} \left[ \frac{f}{20kHz} \right]^2$$

$$x \left[ \frac{n_o}{10^4} \right]^{1/2} \left[ \frac{MHz}{f_o} \right]^{3/2} \left[ \frac{L_z}{5km} \right]^{1/2} x$$

$$x \left[ \frac{P}{10MW} \right] \gamma$$

which is many tens of db above noise. Our preliminary results indicate that this is an extremely important and efficient process and should be studied in appropriate depth, both for proof of principle experiments in Alaska as well as for practical Navy communications.

# Appendix I

## "Generation of ELF/ULF Waves in the Ionosphere by Dynamo Processess

K. Papadopoulos and C.L. Chang

GEOPHYSICAL RESEARCH LETTERS, VOL. 12, NO. 5, PAGES 279-282, MAY 1985

# GENERATION OF ELF/ULF WAVES IN THE IONOSPHERE BY DYNAMO PROCESSES

K. Papadopoulos and C.L. Chang

Science Applications International Corporation

Abstract. It is shown that amplitude modulated HF heating in the ionospheric E-region, can produce substantial power in the ELF/ULF range even in the absence of ambient ionospheric currents. The signals are associated with spontaneous generation of magnetic fields caused by the coupling of the hot spot temperature gradient to the ambient ionospheric density gradient ($\nabla n \times \nabla T$). The mechanism produces values for PC5 micropulsations consistent with those observed by Stubbe and Kopka (1981).

## Introduction

Excitation of VLF/ELF/ULF waves by the interaction of powerful HF waves in the ionosphere has been a very active theoretical and experimental topic. Up to now the most successful excitation techniques have been modulation of the polar and equatorial electrojets. In this technique an HF wave with a frequency of a few MHz is strongly absorbed in the lower ionosphere, resulting in an instantaneous increase in the electron temperature T. The dominant energy loss process, excitation of rotational $N_2$ levels, is also very fast (i.e. less than 1 msec), resulting in instantaneous temperature relaxation, when the HF power is reduced. Transmission of an amplitude modulated HF wave results in oscillation in the electron temperature followed by corresponding oscillation in the conductivity tensor. If the HF heating occurs in ionospheric regions where ambient d.c. currents flow, an a.c. current is generated in the heated volume which radiates at the modulation frequency [Chang et al. 1981, Stubbe et al. 1981]. In this letter we demonstrate that the presence of a d.c. current is not necessary and a substantial a.c. current at the modulated frequency can be spontaneously generated by a dynamo process. The efficiency of the process is inversely proportional to the low frequency. It is also suggested that this process rather than current modulation is the source of the PC5 pulsations received by Stubbe and Kopka (1981) during ionospheric heating experiments.

## Generation of Oscillatory Magnetic Field

Spontaneous generation of magnetic fields from the interaction of electromagnetic (em) waves with plasmas was demonstrated by Stamper et al. (1971) in a laser-plasma interaction experiment. A simple equation was derived in this paper for the spontaneously created magnetic field $\underline{B}$ in the form of

$$\frac{\partial \underline{B}}{\partial t} + \nabla \times \left[ \frac{c^2}{4\pi\sigma} (\nabla \times \underline{B}) \right] - B_o c \nabla \times \left[ \frac{\hat{e}_z \times (\nabla \times \underline{B})}{4\pi ne} \right] - \nabla \times (\underline{u} \times \underline{B}) = \frac{c}{en} (\nabla n \times \nabla T) \quad (1)$$

In Eq. (1) n is the electron density, $\underline{u}$ is the plasma flow velocity, $\sigma$ the conductivity, and the ambient magnetic field was taken as $\underline{B}_o = \hat{e}_z B_o$. The source term on the r.h.s. of Eq. (1) represents a dynamo current due to the presence of a density gradient perpendicular to the temperature gradient. It is obvious from Eq. (1) that in the presence of a stationary density gradient ($\nabla n$) and an oscillatory temperature T the spontaneously generated magnetic field will have a similar time dependence phase shifted by $\pi/2$; therefore, the heated region will act as a radiating antenna. It is not difficult to solve Eq. (1) including the diffusion as well as the Hall and convection terms. It is, however, obvious that for a low $\beta$-plasma ($\beta$ defined as the ratio of plasma pressure to magnetic pressure) the convective term can be neglected. In addition, since this letter addresses only the feasibility of the process and not the details of the radiation pattern, we consider the simple case where the ambient magnetic field $\underline{B}_o$ is parallel to the density gradient $\nabla n$; this corresponds to the experimental configuration in the auroral zones. The azimuthal ($B_\theta$) component of Eq. (1), is then given by

$$\frac{\partial B_\theta}{\partial t} - K \nabla^2 B_\theta = \frac{c}{en} (\nabla n)_z (\nabla T)_r \quad (2)$$

where $K = c^2/4\pi\sigma$ is the magnetic diffusivity in the ambient plasma.

In order to provide quantitative estimates of the amplitude $B_\theta$, we assume cylindrical symmetry about the z-direction and prescribe the source term in Eq. (2) as

$$S(r,z,t) = \frac{c}{en} (\nabla n)_z (\nabla T)_r =$$

$$= \frac{S_o}{2} \exp\left[ - \frac{r^2}{L_T^2} \right] \exp\left[ - \frac{z^2}{L_Z^2} \right] [1-\cos(\omega t)] \quad (3a)$$

where

$$S_o = \frac{c}{e} \frac{1}{L_N} \frac{\tilde{T}}{L_T} \quad , \quad (3b)$$

$L_N = [(\nabla n)_z / n]^{-1}$ is the ambient density gradient length, $\tilde{T}/L_T$ is the volume averaged temperature gradient in the HF heated plasma, and $L_Z$ represents the characteristic dimension of the heated region in the vertical direction.



Paper Number 5L6435
0094-8276/85/005L-6435$03.00

The cylindrically symmetric version of Eq. (2) with the source term given by Eqs. (3) can be solved as generalized diffusion equations by using a combination of Fourier-Bessel transforms. Following the procedure outlined in the appendix (Eq. A5) we find

$$B_\theta(r,z,t) = \frac{S_o}{2\omega}\int_o^\tau d\tau' \frac{(1-\cos\tau')\exp\left[-\frac{(r/L_T)^2}{D(\tau-\tau')}\right]\exp\left[-\frac{(z/L_Z)^2}{F(\tau-\tau')}\right]}{(D(\tau-\tau'))\ (F(\tau-\tau'))^{\frac{1}{2}}} \quad (4)$$

where $\tau=\omega t$, $\tau'=\omega t'$ and

$$D(\tau-\tau') = \frac{4K}{\omega L_T^2}(\tau-\tau')+1 \quad (5a)$$

$$F(\tau-\tau') = \frac{4K}{\omega L_Z^2}(\tau-\tau')+1 \quad (5b)$$

The amplitude of the spontaneously generated magnetic field $B_\theta$ will be controlled by the values of $4K/\omega L_T^2$ and $4K/\omega L_Z^2$. These parameters correspond to the ratio of the radial and axial diffusion time scales $L_T^2/K$ and $L_Z^2/K$ to the ELF/ULF time scale $4/\omega$. They represent the balancing between magnetic field dissipation due to the diffusion term in Eq. (2) and the magnetic field generation due to the source term. Equation (4) has simple solutions in the limiting cases of $4K/\omega(L_T^2, L_Z^2) >> 1$ and $4K/\omega(L_T^2, L_Z^2) << 1$. In the first case the diffusion time through the modified region is short compared to the ELF/ULF time scale ($4/\omega$) and limits the amplitude to

$$B_\theta(0,0,t) = \frac{S_o}{16K}[\min(L_T^2,L_Z^2)][1-\cos(\omega t)] \quad (6)$$

Eq. (6) was found by approximating the time integration by taking the most significant contribution from the integrand at $\tau'=\tau$ and multiplying by the width of the contributed part [min $(L_T^2,L_Z^2)$] $\omega/8K$. This simply states the physically obvious conclusion that the field amplitude is $S_o\tau_{diff}$, where $\tau_{diff}$ is the minimum axial or radial diffusion time through the modified region.

The second limit corresponds to long diffusion time $\tau_{diff}$ relative to the ELF/ULF build up time $4/\omega$. The value of $B_\theta$ found by performing the time integration in the limit that $k\to 0$ is

$$B_\theta(0,0,t) = \frac{S_o}{2\omega}[\omega t-\sin(\omega t)] \quad (7)$$

## ULF Generation in the Lower Ionosphere

In this letter we will concentrate on the limit of long diffusion times, which for the frequenices under consideration is applicable in the lower ionosphere. The situation described by Eq. (6) as well as intermediate cases will be discussed in a future publication.

From Eq. (7), we can see that the spontaneously generated magnetic field consists of two parts. A steady magnetic field buildup increasing linearly with time due to zero diffusivity, and an oscillatory piece due to temperature modulation. The amplitude of the oscillatory magnetic field is $S_o/2\omega$, and in practical units, will be given by

$$|\tilde{B}(r,z,t)| = 10^{-1}\left[\frac{Hz}{f}\right]\left[\frac{\tilde{T}}{1000°K}\right]\left[\frac{10km}{L_N}\right]\left[\frac{10km}{L_T}\right]\gamma \quad (8)$$

An important result of Eq. (8) is the scaling of the field amplitude as 1/f. Stubbe and Kopka (1981) detected a B field amplitude of 10.8Y for 10 min. and 5.4$\gamma$ for 5 min. period micro-pulsations excited by heating, which is consistent with the 1/f dependence of Eq. (8). Notice that if we take $\tilde{T} \approx 10^3$K, $L_N \approx L_T \approx 10$ km which corresponds to expected experimental values, we find from Eq. (8) $B_\theta \approx 5\gamma$ for f = .02 Hz (T = 5 min.) and $B_\theta \approx 10\gamma$ for f = .01 Hz. As mentioned by Stubbe and Kopka (1981) the power expected on the basis of current modulation for the PC5 frequencies is by two orders of magnitude smaller. In comparing the estimates of Eq. (8) with the observations on the ELF-VLF range it is clear that the 1/f dependence does not hold for the range above 200 Hz and that the values expected from Eq. (8) are much lower than the ones expected on the basis of current modulation. For example for f = 2kHz, Eq. (8) predicts $10^{-4}\gamma$ at the source which is much smaller than the value of $10^{-3}\gamma$ measured on the ground. On the other hand the values detected near and below 10 Hz are consistent with the observed. On the basis of the above we expect that the transition from current modulation to dynamo action being the dominant process occurs in the range between 10-200 Hz. We note that inclusion of the Hall term in Eq. (1) does not affect the total magnetic field energy produced by dynamo action; the Hall term simply redistributes the $B_\theta$ generated flux to $B_r$ and $B_z$ components. For the E-region and $L_T \approx$ 10km the long diffusion time approximation is restricted to frequenices f > .01Hz. Below this frequency field saturation described by Eq. (6) occurs.

## Power Estimates

From Eq. (7) we find that the power radiated in the low frequency wave is

$$P_{LF} = \frac{1}{2}\pi L_T^2 L_N \frac{\partial}{\partial t}\frac{B_\theta^2}{4\pi} = \frac{1}{8}\frac{c^2\tilde{T}^2}{e^2 L_T}\frac{1}{\omega} \quad (9)$$

which in practical units becomes

$$P_{LF} \approx .3\left[\frac{\tilde{T}}{10^3°K}\right]^2\left[\frac{10km}{L_T}\right]\left[\frac{1Hz}{f}\right] W \quad (10)$$

Since values of $\tilde{T}$ of the order of 4-5 $\times 10^3$°K can easily be obtained, radiating power of the order of several tens of Watts can be generated in the ULF and lower ELF range. Such temperatures require powers of 1-2 MW [Perkins and Roble 1978; Chang et al. 1981]. Optimization of the scheme

Our starting point for the derivation of the nonlinear currents that couple the three modes is [*Gurevich*, 1977; *Perkins and Goldman*, 1981] the warm collisional electron fluid equations

$$\left[\frac{\partial}{\partial t} + \mathbf{v}_e \cdot \nabla\right] \mathbf{v}_e = -\frac{e}{m_e}\left[\mathbf{E} + \frac{\mathbf{v}_e \times \mathbf{B}}{c}\right] - \nu \mathbf{v}_e - \frac{\nabla p_e}{m_e n_e} \tag{8}$$

$$\left[\frac{\partial}{\partial t} + \mathbf{v}_e \cdot \nabla\right] n_e = -n_e \nabla \cdot \mathbf{v}_e \tag{9}$$

$$\left[\frac{\partial}{\partial t} + \mathbf{v}_e \cdot \nabla\right] T_e = \frac{2}{3}(\nu m_e \mathbf{v}_e - T_e \nabla) \cdot \mathbf{v}_e - \Delta\nu (T_e - T_o) \tag{10}$$

which together with the equation of state for the pressure $p_e = n_e T_e$, form a closed system of equations for $n_e$, $\mathbf{v}_e$, $T_e$; $\cdot\ \Delta\nu$ is the mean fraction of energy lost per collision, and $T_o$ the ambient temperature. In (10) we have neglected heat conduction, an assumption valid for the *E* but not for the *F region*. Other therms neglected, such as friction and thermal force, do not change the final results. The nonlinear currents can be computed by considering small perturbations about a nondrifting equilibrium ($n_o$, $T_o$) so that $\mathbf{v}_e = \mathbf{v}$, $n_e = n_o + n$, $T_e = T_o + T$, assuming plane wave solutions of the form $\exp[-i(\omega t - \mathbf{k}.\mathbf{i})]$ and using the resonance conditions

$$\begin{aligned} \omega_1 &= \omega_2 + \omega_3 \\ \mathbf{k}_1 &= \mathbf{k}_2 + \mathbf{k}_3 \end{aligned} \tag{11}$$

The computation is tedious but straightforward and is given in the appendix. The resulting high-frequency nonlinear

$$\epsilon_3^{xx} = \frac{\omega_{pi}^2}{\omega_{ci}^2} \left(1 + i \frac{\nu_3}{\omega_3}\right) \tag{5a}$$

$$\epsilon_3^{xy} = 0 \tag{5b}$$

which allows propagation of Alfven waves as long as $\nu_3/\omega_3 \ll 1$.

(2) For $\omega_3 \gg \omega_{ci}, \nu_3$

$$\epsilon_3^{xx} = 0 \tag{6a}$$

$$\epsilon_3^{xy} = -\frac{i\omega_{pe}^2}{\omega_{ce}\omega_3} \tag{6b}$$

which is the usual electron whistler.

(3) For $\nu_3 \gg \omega_{ci}, \omega_3$

$$\epsilon_3^{xx} = 0 \tag{7a}$$

$$\epsilon_3^{xy} = -i \frac{\omega_{pe}^2}{\omega_{ce}\omega_3} \tag{7b}$$

regardless of the $\omega_3/\omega_{ci}$ ratio. This is similar to the whistler dispersion found above for $\omega_3 > \omega_{ci}$; it is the helicon mode (Menyuk, Ko, and Papadopoulos, manuscript in preparation, 1984). In this case, contrary to case (1) above, the current is carried by the electrons while the ions are viscously frozen. In this sense it is analogous to the well-known helicon wave in solid state physics [Aigrain, 1961] in which the current is carried by the free electrons, while the ion motion is frozen by the lattice. Referring to the excitation of ELF waves below 100 Hz in the lower ionosphere it is obvious that the relevant mode is the helicon rather than the Alfven mode, to which we shall restrict our attention.

low-frequency wave is then [Krall and Trivelpiece, 1973]

$$\begin{bmatrix} \frac{\omega_3^2}{c^2}\,\epsilon_3^{xx} - k_{3z}^2 & \frac{\omega_3^2}{c^2}\,\epsilon_3^{xy} \\ -\frac{\omega_3^2}{c^2}\,\epsilon_3^{xy} & \frac{\omega_3^2}{c^2}\,\epsilon_3^{xx} - k_3^2 \end{bmatrix} = 0 \qquad (2)$$

where $\epsilon_3^{xx}$ and $\epsilon_3^{xy}$ are the diagonal and the off-diagonal elements of the cold plasma dielectric tensor. Assuming $\omega_{ce} \gg \nu \gg \omega_3$ we find

$$\epsilon_3^{exx} = i\,\frac{\omega_{pe}^2}{\omega_{ce}^2}\,\frac{\omega_3}{\nu} \qquad \epsilon_3^{exy} = -i\,\frac{\omega_{pe}^2}{\omega_{ce}\omega_3} \qquad (3a)$$

$$\epsilon_3^{ixx} = \frac{\omega_{pi}^2\,(\omega_3 + i\nu_3)}{\omega_3\left[\omega_{ci}^2 - (\omega_3 + i\nu_3)^2\right]} \qquad \epsilon_3^{ixy} = \frac{i\omega_{pi}^2\,\omega_{ci}}{\omega_3\left[\omega_{ci}^2 - (\omega_3 + i\nu_3)^2\right]} \qquad (3b)$$

For $\omega_{pi}^2 \gg \nu, \max(\omega_{ci}, \nu_3, \omega_3)$, equations (3) reduce to

$$\epsilon_3^{xx} = 1 + \epsilon_3^{exx} + \epsilon_3^{ixx} = \frac{\omega_{pi}^2}{\left[\omega_{ci}^2 - (\omega_3 + i\nu_3)^2\right]}\,\frac{\omega_3 + i\nu_3}{\omega_3} \qquad (4a)$$

$$\epsilon_3^{xy} = \epsilon_3^{exy} + \epsilon_3^{ixy} = -i\,\frac{\omega_{pe}^2}{\omega_{ce}\omega_3}\left[1 - \frac{(\omega_3 + i\nu_3)^2}{\omega_{ci}^2}\right]^{-1} \qquad (4b)$$

From (2) and (4) and neglecting the displacement current we find the following regimes of weakly attenuated proper eigenmodes:

(1) For $\omega_{ci} \gg \omega_3, \nu_3$

compute the power and electric field threshold conditions for ELF generation in the lower ionosphere by two HF pumps under steady state conditions and to discuss the antenna requirements for a proof of principle experiment. The final section summarizes our results, stresses their limitations, and outlines potential improvements and extensions.

## 2. NONLINEAR INTERACTION OF TWO HF WAVE PACKETS WITH AN ELF WAVE IN THE LOWER IONOSPHERE

We assume first that the two interacting high-frequency waves have $\omega_1$, $\omega_2 \gg \omega_{ce}$, where $\omega_{ce}$ is the electron cyclotron frequency. In this case the plasma behaves isotropically, so that the dielectric tensors $\epsilon_{1,2}$ of the two waves are diagonal, i.e., $\epsilon_{1,2}$ I. In the fluid approximation the dispersion relation is then

$$D_{1,2} = \frac{\omega_{1,2}^2}{c^2} \epsilon_{1,2} - k_{1,2}^2 = 0 \qquad (1a)$$

$$\epsilon_{1,2} = 1 - \frac{\omega_{pe}^2}{\omega_{1,2}^2} \left[ 1 - i \frac{\nu}{\omega_{1,2}} \right] \qquad (1b)$$

where $\omega_{pe}$ is the plasma frequency and $\nu$ the electron-neutral collision frequency. For the low-frequency wave we consider $\omega_3 < \omega_{pi}$, where $\omega_{pi}$ is the ion plasma frequency, so that we can neglect its electric field parallel to the ambient magnetic field, whose direction is taken along the z axis (i.e., $E_{3z} \approx 0$). The dispersion relation for the

Gurevich, 1978] dominates over the ponderomotive force, the downconversion efficiency is increased by a factor $\nu/\omega_3$ where $\nu$ is the electron collision frequency. Furthermore the power threshold required for complete decay is reduced by a comparable $\nu/\omega_3$ factor. Since the values of $\nu$ are larger for the lower ionosphere (i.e., E region), it is advantageous to consider the interaction in this region.

In this paper we examine the ELF generation in the ionospheric E region by the beating of two HF heaters. In the next section we discuss the ELF plasma eigenmodes in the E region where the two HF pumps will couple and derive the equations describing the nonlinear interaction of the three wave packets. It is noted that for altitudes below 150 km the ion-neutral collision frequency ($\nu_3$) is larger than the ion cyclotron frequency ($\omega_{ci}$), thereby not allowing the existence of proper Alfven or magnetosonic eigenmodes. It is then found that the viscous ion damping ($\nu_3 > \omega_{ci}$) freezes the ion motion and allows the whistler mode to continue as a helicon [Aigrain, 1961] a right-and polarized mode, to frequencies $\omega_3 < \nu_3$. In Section 3, we extend the work performed on threshold conditions and power transfer efficiency in collisionless three wave packet interactions to the collisional regime. This section includes many novel and rather profound physical issues. Section 4, uses the mathematical and numerical conclusions of Section 3, to

nonlinear mechanisms for ELF generation which are independent of the ambient current. *Papadopoulos et al.* [1982] considered the possibility of parametric excitation of an Alfven or magnetosonic wave in the ionosphere by beating two high-frequency waves ($\omega_1$, $\omega_2$) with $\omega_1-\omega_2$ equal to the frequency of the low-frequency mode ($\omega_3$). The process envisioned was essentially a modified stimulated forward Brillouin scattering [*Liu*, 1976] with the Alfven wave, instead of an ion acoustic wave, acting as the low-frequency signal. In the language of parametric instabilities the pump ($\omega_1$) and the idler ($\omega_2$) are HF waves, while the signal ($\omega_3$) was an Alfven or magnetosonic mode. In the work by *Papadopoulos et al.* [1982] the process was considered as collisionless so that the ponderomotive force was the dominant nonlinear force. The power threshold necessary for complete decay can be found by the inverse scattering transform (IST) method [*Zakharov and Manakov*, 1975; *Reiman*, 1977; *Kaup et al.*, 1979] The analysis revealed that for upper F region ionospheric parameters the power threshold necessary to excite Alfven waves was very large. In addition the maximum downconversion efficiency was limited by the Manley-Rowe relations [*Sagdeev and Galeev*, 1969] to $\omega_3/\omega_1$, i.e., less than $10^{-4}$ for downconverting 5 MHz to 100 Hz. It was subsequently noted [*Papadopoulos et al.*, 1983] that if the thermal nonlinearity caused by collisional electron heating [*Berger et al.*, 1975;

Due to technical problems with the Tromso heating facility it has not been possible to generate signals in the 10-Hz to 200-Hz regime. However, signals up to 10 $\gamma$ have been generated for Pc 5 pulsations up to 10 Hz. These signals are much larger than expected from current modulation, and their physical origin has been a mystery. In a recent paper, *Papadopoulos and Chang*, 1985 noted that spontaneously generated magnetic fields with time variation similar to the HF modulation can be generated during ionospheric heating experiments when $\nabla n \times \nabla T_e \neq 0$, where $\nabla n$ is the ambient ionospheric density gradient and $\nabla T_e$ the electron temperature gradient in the heated region. The generation of these fields is independent of the ambient current, and its physical origin has been demonstrated in laser-produced plasmas [Stamper *et al.*, 1971]. *Papadopoulos and Chang* [1985] indicate that for frequencies below 40 Hz the spontaneous field generation dominates over the current modulation, thereby explaining the large observed signals.

While the above mechanisms appear to be rather well understood, they are relatively inefficient in downconverting HF power to ELF. In addition the nonlinear demodulation can be applied only in regions of preexisting currents, and the maximum generated signal amplitude is strictly constrained by the local current values. These limitations provoked the search for other more efficient

waves amplitude modulated at the desired low frequency. The basic physics of the technique, known as nonlinear demodulation or, for historical reasons, ionospheric detection, lies in the fact that the HF wave produces modulated electron heating, which results in modulation of the local conductivity. Natural ionospheric currents which pass through the illuminated region are modulated by the conductivity changes, producing a radiating dipole current pattern [*Chang et al.*, 1981]. The earliest experimental results on nonlinear demodulation were observed during the Soviet heating experiments at Gorkii [*Germantsev et al.*, 1973; *Kapustin et al.*, 1977]. The polar electrojet was modulated in the VLF range (1–7 kHz) with a 5.75-MHz carrier and 15-MW effective radiative power (ERP). Signals were observed only between 2.5 and 4 kHz with strength in the range 2–25 x $10^{-2}$ $\mu$V/m. More reliable results for polar electrojet modulation were reported by the Max Planck group [*Stubbe et al.*, 1982a, b] using the Tromso Norway ionospheric heater. The ERP in this case varied between 75 and 125 MW, and the HF frequency utilized was 2.5–8 MHz. VLF signals with amplitude $10^{-3}$ $\gamma$ were observed with maxima for 2 kHz. Finally *Ferraro et al.* [1982] reported VLF signals in the 500-Hz to 5-kHz range using the Arecibo HF heater at 3.17 MHz to modulate the equatorial electrojet. Again maximum strength appeared for 2-kHz VLF signals.

## 1. INTRODUCTION

The interaction of high-power radio waves with the ionospheric plasma is strongly nonlinear. The main nonlinearities arise through the ponderomotive and thermal forces. As a result of the nonlinear interactions, electrostatic (es) and electromagnetic (em) waves with frequencies different than the pump frequency can be generated. A comprehensive review of the subject can be found in a recent monograph [*Gurevich*, 1978]. The present paper examines the feasibility and the efficiency of utilizing the nonlinearities of the ionospheric plasma to downconvert HF signals to ELF in a controlled fashion. The subject matter, besides its intrinsic scientific merit, has a broad spectrum of applications, ranging from ionospheric and magnetospheric probing to low-frequency submarine communications. The emphasis in this work will be on the nonlinear physics aspects of the interaction, the projected scalings, and the heater requirements for a proof of principle experiment.

Ionospheric heaters have been used successfully for the generation of VLF and ULF signals [*Stubbe* and *Kopka* 1977; *Stubbe et al.*, 1981; *Ferraro et al.*, 1982]. These experiments induced local modulation of existing ionospheric currents, such as the auroral and equatorial electrojets, by illuminating the current-carrying region with strong HF

Generation of ELF waves by stimulated parametric couplins of two HF waves in the lower ionosphere is considered. In this resion the nonlinear force is dominated by the thermal rather than the ponderomotive nonlinearity. It is shown that this results in lowerins the pump threshold for complete decay by more than an order of masnitude while achievins efficiencies in excess of those expected on the basis of the Manley-Rowe relations. The lower-frequency mode excited for E resion altitudes is the helicon mode, which continues to frequencies below the ion cyclotron frequency because ion-neutral collisions freeze the ion motion. The application of these results to ELF seneration in the lower ionosphere, includins power estimates for a proof of principle experiment, is discussed.

# ELF Generation In The Lower Ionosphere Via Collisional Parametric Decay

K. KO, C.R. MENYUK, REIMAN, V. TRIPATHI,

P. PALMADESSO, AND K. PAPADOPOULOS

## Appendix II

"ELF Generation in the Lower Ionosphere
via Collisional Parametric Decay

K. Ko, C.R. Menyuk, A. Reiman, V. Tripathi,
P. Palmadesso, and K. Papadopoulos

Stubbe, P. and H. Kopka, Generation of Pc5 pulsations by polar electrojet modulation, J. Geophys. Res., 86, 1606-1608, 1981.

Stubbe, P., H. Kopka, and R.L. Dowden, Generation of ELF and VLF waves by polar electrojet modulation, J. Geophys. Res., 86, 9073-9078, 1981.

K. Papadopoulos and C.L. Chang, Science Applications International Corporation, McLean, VA 22102

(Received January 9, 1985;
Accepted January 30, 1985)

requires maximizing the electron temperatures ($T^2$ dependence) while minimizing the heated area ($1/L_H$ dependence). Both can be achieved with high antenna gain and by optimizing the energy deposition altitude. Detailed numerical studies are in progress and will be reported elsewhere.

## Summary and Discussion

We have shown that amplitude modulated ionospheric heating can generate spontaneous magnetic fields by coupling to the density gradients of the ionospheric plasmas. The time dependence of the spontaneous magnetic fields is similar to the dependence of the temperature gradient perpendicular to the ionospheric temperature gradient, shifted by $\pi/2$ in phase. Therefore a periodic heating pulse will generate periodic magnetic pulsation. The amplitude and power of the low frequency signal scales of 1/f favoring the lower frequency signals. It is important to note that the mechanism does not require and is not affected by the presence of ambient ionospheric currents. The field generation is due to the presence of a source term producing fields with $\nabla \times \underline{E} \neq 0$ and is not a plasma or parametric instability such as discussed by Kuo and Lee (1983). In this paper we demonstrated the basic physical mechanism along with approximate estimates of the expected amplitude and power. It is easy to show that short scale density fluctuations due to ponderomotive force or density modulation will not affect the zero order field generation. The role of diffusion as well as application and scaling of the process for situations that $\nabla n$ is at angle to $\underline{B}_o$, are presently under study and will be reported elsewhere.

## Appendix

For cylindrical symmetry, such as expected in the HF heating experiment, Eq. (2) reduces to

$$\left\{\frac{\partial}{\partial t} - K\left[\frac{1}{r}\frac{\partial}{\partial r}\left[r\frac{\partial}{\partial r}\right] + \frac{\partial^2}{\partial z^2}\right]\right\} B_\theta(r,z,t) = S(r,z,t) \tag{A1}$$

where $S(r,z,t)$ is an arbitrary time dependent source given by Eqs. (3). Introducing a Bessel transform in r, and a Fourier transform in z, such as

$$B_\theta(\ell,k,t) = \frac{1}{2\pi}\int_0^\infty dr\, r \int_{-\infty}^{\infty} dz\, B_\theta(r,z,t) J_o(\ell r) e^{-ikz} \tag{A2}$$

equation (A1) reduces to

$$\left[\frac{\partial}{\partial t} + K(\ell^2+k^2)\right] B_\theta(\ell,k,t) = S(\ell,k,t) \tag{A3}$$

This equation is first order in time and yields an exact solution

$$B_\theta(\ell,k,t) = B_\theta(\ell,k,o)e^{-(\ell^2+k^2)Kt} + \int_o^t dt' S(\ell,k,t') e^{-(\ell^2+k^2)K(t-t')} \tag{A4}$$

where $B_\theta(\ell,k,o)$ is the Fourier-Bessel component of the initial condition $B_\theta(r,z,o)$ at $t = 0$. Final solution of Eq. (A1) is then obtained by the inverse transform

$$B_\theta(r,z,t) = \int_o^\infty d\ell\, \ell \int_{-\infty}^{\infty} dk\, B_\theta(\ell,k,t)\, J_o(\ell r) e^{ikz} \tag{A5}$$

Note that this procedure leaves the form of source term $S(r,z,t)$ unspecified, and can be extended to include the azimuthal dependence of the problem by adding a $\theta$ transform $\int d\theta\, e^{im\theta}$.

For the source term given by Eqs. (3) and $B_\theta(r,z,o)=0$, Eq. (A5) gives

$$B_\theta(r,z,t) = \frac{S}{2\omega}\int_o^\tau d\tau(1-\cos\tau') \exp\left\{-\left[\frac{(r/L_r)^2}{\frac{4K}{\omega L_r^2}(\tau-\tau')+1}\right]\right\} \exp\left\{-\left[\frac{(z/L_z)^2}{\frac{4K}{\omega L_z^2}(\tau-\tau')+1}\right]\right\} \Big/ \left[\frac{4K}{\omega L_r^2}(\tau-\tau')+1\right]\left[\frac{4K}{\omega L_z^2}(\tau-\tau')+1\right]^{1/2} \tag{A6}$$

where $\tau = \omega t$, $\tau' = \omega t'$ and the integral relations

$$\int_o^\infty dr\, r e^{-(r/L_r)^2} J_o(\ell r) = \frac{L_r^2}{2} e^{-(L_r\ell/2)^2}$$

$$\int_{-\infty}^{\infty} dz\, e^{-ikz} e^{-(z/L_z)^2} = \sqrt{\pi}\, L_z e^{-(L_z k/2)^2} \tag{A7}$$

were used to obtain the final result.

Acknowledgments. We would like to express our thanks to Dr. A.T. Drobot for many valuable discussions, and to Dr. C. Menyuk for his scrutiny of much of this letter. This work was supported by ONR under Contract No. N00014-84-C-0353.

## References

Chang, C.L., V. Tripathi, K.Papadopoulos, J. Fedder, P.J. Palmadesso, and S.L. Ossakow, Wireless generation of ELF/VLF radiation in the ionosphere in Effects of the Ionosphere on Radiowave Systems edited by J.M. Goodman, Ionospheric Effects Symposium sponsored by NRL, ONR, and AFGL, pp. 91-99, 1981.

Kuo, S.P. and H.C. Lee, Earth magnetic field fluctuations produced by filamentation instability of electromagnetic heater waves, Geophys. Res. Lett., 10, 979-981, 1983.

Perkins, F.W. and R.G. Roble, Ionospheric heating by radiowaves, J. Geophys. Res., 83, 1611-1624, 1978.

Stamper, J.A., K. Papadopoulos, R.N. Sudan, S.O. Dean, E.A. McLean, and J.M. Dawson, Spontaneous magnetic fields in laser produced plasmas, Phys. Rev. Lett., 26, 1012-1014, 1971.

currents are

$$J_1^{NL} = -\frac{e}{4\pi m_e}\frac{E_2}{\omega_2}\left(1-\frac{e\nu}{\omega_2}\right)(k_3\cdot\epsilon_3^e\cdot E_3)$$
$$J_2^{NL} = \frac{e}{4\pi m_e}\frac{E_1}{\omega_1}\left(1-\frac{i\nu}{\omega}\right)(k_3\cdot\epsilon^e\cdot E_3)^* \qquad (12)$$

Here and in the rest of the paper, $v$, $n$, $T$, $J$, and $E$ are Fourier-transformed quantities. With the exception of the small $i\nu/\omega_{1,2}$ terms, (12) is the standard result [*Weiland and Wilhelmson*, 1977]. The low-frequency nonlinear current is given by

$$J_3^{NL} = \frac{e}{4\pi m_e}\frac{\omega_3}{\omega_1\omega_2}\,\epsilon_3^e\cdot k_3\,(E_1\cdot E_2^*)\left(1+i\frac{4\nu}{3\omega}\right)_3 \qquad (13)$$

For $\nu=0$ this is again nothing more than the standard low-frequency current caused by the collisionless ponderomotive force [*Papadopoulos et al.*, 1982]. The coefficient $4\nu/\omega_3$ is due to the nonlinear perturbation caused by Ohmic heating. For $\nu/\omega_3 \gg 1$ it becomes the dominant term, introducing a $\nu/\omega_3$ enhancement factor in the current as well as a $\pi/2$ phase shift. Several physical comments on the derivation of (12) and (13) can be found in the appendix.

Using the currents $J^{NL}$ as a source in the wave equation for each of the three waves we find

$$D_j \cdot E_j = -\frac{i4\pi\omega_j}{c^2} J_j^{NL}$$

$$D_j = \frac{\omega_j}{c^2} \epsilon_j - k_j^2 I + k_i k_i \qquad (14)$$

In the absence of nonlinear currents ($J^{NL} = 0$) the vanishing of the determinants, $|D_j| = 0$, represents the linear dispersion relations of the individual waves, that were given by (1) and (2). Taking without loss of generality the polarizations of $E_{1,2}$ as

$$E_{1,2} = E_{1,2}\, y \qquad (15)$$

and using the isotropic property of the tensors $\epsilon_{1,2}$ for $\omega_{1,2} >> \omega_{ce}$, we find

$$D_1 E_1 = -i \frac{4\pi\omega_1}{c^2} J_1^{NL}$$

$$D_2 E_2 = -i \frac{4\pi\omega_2}{c^2} J_2^{NL} \qquad (16)$$

with $D_{1,2}$ given by (1) and $J_{1,2}^{NL}$ by (12). For the polarization given by (15) and using the fact that $E_{3z} \approx 0$ for $\omega_3 << \omega_{pi}$, the equations for the low-frequency wave are given by

$$\left[ \frac{\omega_3^2}{c^2} \epsilon_3^{xx} - k_{3z}^2 \right] E_{3x} + \frac{\omega_3^2}{c^2} \epsilon_3^{xy} E_{3y} = -\frac{i4\pi\omega_3}{c^2} J_{3x}^{NL} \qquad (17a)$$

$$-\frac{\omega_3^2}{c^2} \epsilon_3^{xy} E_{3x} + \left[ \frac{\omega_3^2}{c^2} \epsilon_3^{xx} - k_3^2 \right] E_{3y} = -\frac{i\pi\omega_3}{c^2} J_{3y}^{NL} \qquad (17b)$$

where $\epsilon_3^{xx}$ and $\epsilon_3^{xy}$ are given by Eqs. (4). Eliminating $E_{3x}$ from (17), we find

$$D_3 E_{3y} = \frac{-i4\pi\omega_3}{c^2}\left[\frac{\omega_3^2}{c^2}\ \epsilon_3^{xy}\left[\frac{\omega_3^2}{c^2}\ \epsilon_3^{xx} - k_{3z}^2\right]^{-1} J_{3x}^{NL} + J_{3y}^{NL}\right] \quad (18)$$

where

$$D_3 = \left[\frac{\omega_3^2}{c^2}\ \epsilon_3^{xy}\right]^2\left[\frac{\omega_3^2}{c^2}\ \epsilon_3^{xx} - k_{3z}^2\right]^{-1} + \left[\frac{\omega_3^2}{c^2}\ \epsilon_3^{xx} - k_3^2\right] \quad (19)$$

Depending on whether we are coupling to Alfven waves or whistler-helicon waves, the values of $\epsilon_3^{xx}$, $\epsilon_3^{xy}$ will be given by (5) or (7). In this paper we are interested in coupling to helicons, so that

$$|\epsilon_3^{xy}| \ / \ \epsilon_3^{xx} = (m_i/m_e)\ (\nu/\omega_{ce}) \gg 1.$$

Therefore, $D_3$ becomes

$$D_3 = -\frac{\left[k_3 k_{3z} - \frac{\omega_3^2}{c^2}\,|\epsilon_3^{xy}|\right]\left[k_3 k_{3z} + \frac{\omega_3^2}{c^2}\,|\epsilon_3^{xy}|\right]}{k_3^2} \quad (20)$$

with $\epsilon_3^{xy}$ given by (7b). The case of Alfven waves can be examined in an analogous manner. Assuming without loss of generality that $k_{3y} = 0$ we find that $\mathbf{k}_3 \cdot \epsilon_3 \cdot \mathbf{E} = k_{3x}\ \epsilon_3^{xy}\ E_y$, so that $J_3 = J_{3y}\ \mathbf{y}$. From (12), (13), (16), (18), and (20) we find the coupled system of equations,

$$D_1 \frac{E_1}{\omega_1} = \beta\left(1 - \frac{i\nu}{\omega_2}\right)\frac{E_2}{\omega_2}\frac{E_3}{\omega_3} \quad (21a)$$

$$D_2 \frac{E_2}{\omega_2} = \beta\left(1 - \frac{i\nu}{\omega_1}\right)\frac{E_1}{\omega_1}\frac{E_3^*}{\omega_3} \quad (21b)$$

$$D_3 \frac{E_3}{\omega_3} = \beta \left(1 + \frac{i4\nu}{3\omega_3}\right) \frac{E_1}{\omega_1} \frac{E_2^*}{\omega_2} \qquad (21c)$$

where

$$\beta = \frac{e}{mc^2} \frac{k_{3x}\omega_{pe}^2}{\omega_{ce}} \qquad (22)$$

and we have set $E_{3y} = E_3$. In the collisionless case the high-frequency waves produce a low-frequency ponderomotive force, $-eE_3^P$, on the electrons, which results in a nonlinear current $J_3^{NL}$ that drives $E_3$. In the collisional case, $J_3^{NL}$ is predominantly due to a temperature perturbation $T_3^{NL}$ when the electrons are Ohmically heated. In either case, the beating of the high-frequency velocities $v^L{}_1$, $v^L{}_2$ with the low-frequency density perturbation $n_3{}^L$ provides the primary coupling mechanism between $E_3$ and the high-frequency fields $E_1$, $E_2$. It is worth noting that for interaction with $\omega_3 \ll \omega_1, \omega_2$, $|k_3| \ll |k_1|, |k_2|$, and by choosing the HF electric field polarization in the y direciton, we end up with all of the nonlinear currents and the low-frequency electric field in the y direction.

Equations (21) describe the interaction of infinite, homoseneous, plane waves. In practice, however, we deal with two HF wave packets interactins with an ELF wave packet within a spatially localized resion controlled by the antenna sain. In order to determine the efficiency of the interaction the localized and inhomoseneous nature of the

wavepacket interaction should be included. For a weakly nonlinear interaction between localized wave packets, we follow the standard procedure and expand $D_j$ in a Taylor series about the phase matching point where the resonance conditions (11) are met; that is, we let

$$D_j + \frac{i\partial D_j}{\partial \omega_j}\left[\frac{\partial}{\partial t} + \Gamma_j\right] - \frac{i\partial D_j}{\partial k_j}\cdot\nabla + \ldots$$

operate on

$$E_j(r,t) = \mu_j a_j(r,t)\, e^{-i(\omega_j t - k_j\cdot r)} \tag{23a}$$

where

$$\mu_j = \omega_j / (\partial D_j/\partial\omega_j)^{\frac{1}{2}} \tag{23b}$$

and $a_j$ is the slowly varying envelope of the $j^{th}$ wave packet. The linear damping rates $\Gamma_j$ are given by the imaginary parts of $D_j$ while the partial derivatives of $D_j$ are evaluated for a particular mode $(\omega_j, k_j)$. For positive energy waves as is the case here, $\partial D_j/\partial\omega_j > 0$. Using the fact that, to lowest order, the waves obey the linear dispersion relations $D_j = 0$, we obtain the equations for the collisional three-wave coupling in standard form

$$\left[\frac{\partial}{\partial t} + v_1\cdot\nabla + \Gamma_1\right] a_1 = K\left[1 - \frac{i\nu}{\omega_2}\right] a_2 a_3 \tag{24a}$$

$$\left[\frac{\partial}{\partial t} + v_2\cdot\nabla + \Gamma_2\right] a_2 = -K^*\left[1 - \frac{i\nu}{\omega_1}\right] a_1 a_3^* \tag{24b}$$

$$\left[\frac{\partial}{\partial t} + v_3\cdot\nabla + \Gamma_3\right] a_3 = -K^*\left[1 + \frac{i4\nu}{3\omega_3}\right] a_1 a_2^* \tag{24c}$$

where

$$u_j = -\frac{\partial D_j}{\partial \omega_j} \Big/ \frac{\partial D_j}{\partial k_j} \tag{25a}$$

are the group velocities of the waves and

$$K = -i\beta \Big/ \left[ \frac{\partial D_1}{\partial \omega_1} \frac{\partial D_2}{\partial \omega_2} \frac{\partial D_3}{\partial \omega_3} \right]^{1/2} \tag{25b}$$

is the symmetric coupling coefficient for the collisionless interaction. By setting $\partial/\partial t = 0$, one finds the steady state two-dimensional version

$$\left[\frac{\partial}{\partial z} + u_1 \frac{\partial}{\partial x} + \Gamma_1\right] a_1 = K \left[1 - \frac{i\nu}{\omega_2}\right] a_2 a_3 \tag{26a}$$

$$\left[\frac{\partial}{\partial z} + u_2 \frac{\partial}{\partial x} + \Gamma_2\right] a_2 = -K^* \left[1 - \frac{i\nu}{\omega_1}\right] a_1 a_3^* \tag{26b}$$

$$\left[\frac{\partial}{\partial z} + u_3 \frac{\partial}{\partial x} + \Gamma_3\right] a_3 = -K^* \left[1 + \frac{i4\nu}{3\omega_3}\right] a_1 a_2^* , \tag{26c}$$

where the interaction is assumed to evolve in $z$ ($u_{jz} > 0$). The new variables are expressed as follows:

$$a_j = a_j u_{jz}^{1/2} \qquad u_j = u_{jx} / u_{jz} \quad \Gamma_j = \Gamma_j / u_{jz} \tag{27a}$$

and

$$K = K / (u_{1z} u_{2z} u_{3z})^{1/2} \tag{27b}$$

Equations (26) with the definitions (23) and (25), the value of $\beta$ given by (22), and $D_1$, $D_2$, $D_3$ by (1) and (20) form the basic equations of our problem. In the next section we will use them to determine the transfer efficiency during the steady state interaction of the three wave packets.

## 3. THRESHOLD CONDITIONS AND TRANSFER EFFICIENCY FOR THREE WAVEPACKET INTERACTIONS IN DISSIPATIVE SYSTEMS

Before attempting to solve Eqs. (26) for the situation under study, it is worthwhile to review briefly the previous work on the subject, which, due to its rather mathematical nature, might not have reached the ionospheric community. In the collisionless case (i.e. $\nu$=0), the coupling coefficients are symmetric and the set of Eqs. (24) has an infinite set of invariants. This allows for the use of inverse scattering transform techniques (IST) (*Ablowitz et al.*, 1981). The one dimensional version of Eqs. (24) (*Zakharov and Manakov*, 1975; *Reiman*, 1977; *Kaup et al.*, 1979) has been extensively studied in the literature using IST and the results were confirmed by numerical solutions. As noted before, the two dimensional steady state Eqs. (26) are equivalent to the transformed one dimensional space-time equations. Therefore the results of the one dimensional space time problem can be directly applied to our practical problem. An important result of the one dimensional space-time collisionless analysis is the fact that *the threshold value required for pump depletion is equivalent to the pump amplitude required to achieve an absolute instability within its width L* (*Reiman*, 1977).

For collisionless three wave interactions, the

eisenvalue problem which determines the conditions for absolute instability in a rectangular pump is well known (i.e. the backward wave oscillator) (*Bobroff and Haus* 1967). Taking the pump inhomogeneity to be along x, the instability is absolute if

$$v_{2x}\, v_{3x} < 0 \quad , \tag{28a}$$

$$L > \frac{\pi}{2} L_c \quad , \tag{28b}$$

where $L_c = |v_{2x}v_{3x}|^{\frac{1}{2}} / |\gamma_o|$ is the critical width and $|\gamma_o| = |K^* a_1|$ is the uniform medium growth rate. Eq.(28a) requires the decay waves to be oppositely trav ing, while Eq.(28b) defines the pump threshold for the absolute instability to occur within a width L. We demonstrate below that for the strongly collisional case ($\nu/\omega_3 >> 1$) similar considerations apply. Note, however, that since the coupling coefficients are by a factor $\nu/\omega_3$ larger, the required pump levels are smaller by the same factor. In addition the transfer efficiency increases by the same factor. Notice that due to the dissipative nature of the system IST techniques are not applicable so that one has to resort to numerical techniques.

The linear equations for the eisenvalue problem that determine absolute instability when one considers the initial stage of the interaction during which the pump is large, $a_1 >> a_{2,3}$, are given by the one dimensional version

of Eqs. (24b) and (24c). Here only the evolution of the decay waves is important, so that we have

$$\left[\frac{\partial}{\partial t} + v_{2x}\frac{\partial}{\partial x} + \Gamma_2\right] a_2 = -\gamma_o(x)\, a_3^* \left[1 - \frac{i\nu}{\omega_1}\right] \qquad (29a)$$

$$\left[\frac{\partial}{\partial t} + v_{3x}\frac{\partial}{\partial x} + \Gamma_3\right] a_3 = -\gamma_o(x)\, a_2^* \Lambda \qquad (29b)$$

Note that $\gamma_o(x)$ contains the pump inhomogeneity and $\Lambda$ is defined by

$$\Lambda = 1 + \frac{i4}{3}\frac{\nu}{\omega_3} \qquad (30)$$

For the threshold calculation here, we can ignore the small collisional correction on the RHS of Eq. (29a). The linearly coupled system is solved by taking the conjugate of Eq. (29a) and Laplace transforming in time as $e^{pt}$. We then make the substitution

$$(a_2^*, a_3) = \exp\left[-\frac{1}{2}\left[\frac{p+\Gamma_2}{v_{2x}} + \frac{p+\Gamma_3}{v_{3x}}\right]x\right](A_2, A_3) \qquad (31)$$

to obtain

$$\left[\frac{\partial}{\partial x} + \eta\right] A_2 = -\frac{\gamma_o^*(x)}{v_{2x}} A_3 \qquad (32a)$$

$$\left[\frac{\partial}{\partial x} - \eta\right] A_3 = -\frac{\gamma_o(x)}{v_{3x}} A_2 \Lambda \qquad (32b)$$

where

$$\eta = \frac{1}{2}\left[\frac{p+\Gamma_2}{v_{2x}} - \frac{p+\Gamma_3}{v_{3x}}\right] \qquad (33)$$

Equations (32), when subject to the appropriate boundary conditions, form the eigenvalue problem for the growth rate

$\nu$ which may in general be complex.

In the case of a rectangular pump of width $L$,

$$\gamma_o(x) = \begin{cases} \gamma_o & -L/2 \leq x \leq L/2 \\ 0 & \text{otherwise} \end{cases}$$

one may combine (32) inside the pump region to find

$$\left[\frac{\partial^2}{\partial\zeta^2} + q\right] A_3 = 0 \qquad (34)$$

which describes a harmonic oscillator in the normalized coordinate $\zeta = x/\ell_c$ with a potential

$$q = e^{i\theta} - \eta^2\ell^2$$

where

$$\theta = \tan^{-1}\left[\frac{4}{3}\frac{\nu}{\omega_3}\right]$$

The new critical width is given by

$$\ell_c = L_c / |\Lambda|^{1/3} \quad . \qquad (35)$$

Equation (34) readily admits solutions in terms of trigonometric functions to which we apply the boundary conditions that $A_2$ be zero at $-L/2$ and $A_3$ be zero at $L/2$ for $v_{2x} > 0$, $v_{3x} < 0$. This leads to the dispersion relation

$$q^{1/3} \cot (q^{1/3} L/\ell_c) + \eta\ell_c = 0 \quad , \qquad (36)$$

for the normalized growth rate $\eta\ell_c$. We have evaluated (36) numerically in the limit $\nu/\omega_3 \gg 1$ which sets $\theta = \pi/2$ and $|\Lambda| \sim \nu/\omega_3$. Complex eigenvalues are found, which indicates that absolute instability indeed occurs in the collisional regime. The real and imaginary parts of $\eta\ell_c$ for the first

four growing modes are shown in Figures 1a and 1b as a function of the normalized width $L/\ell_C$. For comparison, the results for the collisionless regime ($\nu = 0$; $\theta = 0$, $\Lambda = 1$, $\ell_C \to L_C$) are also plotted; in this case, the growth rates are purely real. From Figure 1a, one finds the threshold condition in the collisional regime to be

$$L > 1.8\ \ell_C \tag{37}$$

For a given width $L$, it is clear that the pump value $a_1$ required to achieve absolute instability for the collisional interaction, is smaller by the factor $\ell_C/L_C = |\Lambda|^{-\frac{1}{3}}$. Thus a reduction in the required pump power $P_1 \propto |a_1|^2$ by the factor $\omega_3/\nu$ is achieved; in the lower ionosphere, this can be more than two orders of magnitude. The specific pump requirements for a steady state interaction relevant to ELF generation will be discussed in a later section.

As noted earlier, a key result due to *Reiman* (1977) for collisionless interactions is that if the threshold conditions (28) are satisfied, the linear stage of the absolute instability will be followed by pump depletion in the nonlinear stage. It has been shown that an absolute instability can also be established in the collisional regime. Furthermore, the pump threshold is much lower than in the collisionless case. This threshold reduction is of great practical interest, especially for applications to ELF

generation. However, an equally important issue is whether the absolute instability would lead to pump depletion and if so, what values of downconversion efficiency can be obtained. We demonstrate below that nonlinear saturation of absolute instabilities by pump depletion indeed occurs for collisional interactions and that downconversion efficiencies higher than those predicted by the Manley-Rowe relations can be reached.

The feature that distinguishes the collisional from the collisionless interaction is the presence of dissipative terms in the coupling coefficients so that the system's action and energy are no longer time invariant. To see this, we obtain from (24) the following relations for the one dimensional space-time evolution

$$\frac{\partial}{\partial t} c_{12} = -\int_{-\infty}^{\infty} dx\left[\Gamma_1|a_1|^2+\Gamma_2|a_2|^2+\frac{4\nu}{\omega_1}|K|Re(a_1^* a_2 a_3)\right], \quad (38a)$$

$$\frac{\partial}{\partial t} c_{13} = -\int_{-\infty}^{\infty} dx\left[\Gamma_1|a_1|^2+\Gamma_3|a_3|^2-\frac{8\nu}{3\omega_3}|K|Re(a_1^* a_2 a_3)\right], \quad (38b)$$

$$\frac{\partial}{\partial t} \mathcal{T} = -\int_{-\infty}^{\infty} dx\left[\omega_1\Gamma_1|a_1|^2+\omega_2\Gamma_2|a_2|^2+\omega_3\Gamma_3|a_3|^2 + \frac{4}{3}\nu|K|Re(a_1^* a_2 a_3)\right] \quad (38c)$$

where

$$c_{12}=\int_{-\infty}^{\infty} dx\left[|a_1|^2+|a_2|^2\right], \quad c_{13}=\int_{-\infty}^{\infty} dx\left[|a_1|^2+|a_3|^2\right] \quad (39a)$$

and

$$T = \sum_{j=1}^{3} {}_j \quad {}_j = \int_{-\infty}^{\infty} dx\, \omega_j |a_j|^2 \qquad (39b)$$

Notice that the value of $\int dx|a|^2$ is nothing more than the wave action (i.e., number of quanta). In the collisionless limit, the sums $c_{12}$ and $c_{13}$ of the actions and the total energy $T$ are time invariant. Equations (38) with zero on the right hand side are commonly referred to as the Manley-Rowe relations. A direct consequence of these relations is the limitation in the downconversion efficiency from the pump ($\omega_1$) to the signal ($\omega_3$) to a value smaller or equal to $\omega_3/\omega_1$. Extensions of these results to the case of weakly dissipative systems with ponderomotive nonlinearity (i.e., $\Gamma_j/\omega_j \ll 1$) rely on the approximate conservation of $c_{12}$, $c_{13}$, and $T$ for them to be solvable by IST. The IST results have been compared with numerical solutions of Eqs. (24) with $\nu = 0$ and found to agree. They give the same $\omega_3/\omega_1$ downconversion efficiency (*Liu*, 1976). In order to examine the effect of the thermal nonlinearity we solve numerically the system of (24) with $\nu \neq 0$ but $\Gamma_j = 0$.

For the sake of simplicity, we limit ourselves to a model problem in one dimensional space-time $(x,t)$. As a comparison, the results for the collisionless interaction with symmetric coupling coefficients are also presented. The frequencies of the waves are chosen according to (11);

for numerical convenience, we pick in arbitrary units: $\omega_1$ = 10.1, $\omega_2$ = 10.0, $\nu$ = 1.2 and $\omega_3$ = 0.1. The initial wave envelopes are rectangular and the decay waves have small amplitudes; specifically, we let $|a_2|/|a_1|=0.01$, $|a_3|=0.0$. Because we have in mind an absolute instability, we also let the decay waves to have opposite velocities $v_{3x} = -v_{2x}$, thus satisfying (28a). The problem is solved in the pump reference frame so that $v_{1x} \approx 0$. The pump threshold condition, (28b) or (37), is met by setting $|a_1| = 1.0$ in the collisionless case; whereas, in the collisional case, $|a_1|=|\Lambda|^{-\frac{1}{2}} =(4\nu/3\ \omega_3)^{-\frac{1}{2}} = 0.25$. With these values, the respective normalized widths are the same, i.e., $L/L_C = L/\ell_C = 3.2$, so that from Figure 1a, one expects a growing mode in both interactions.

Using the above initial conditions, the coupled system of equations (24) is numerically integrated forward in time. Figure 2 shows the time-asymptotic behavior at $t$ = 25.0. We observe that pump depletion occurs in both interactions. In the collisonless case, the decay waves emerge as symmetric pulses. They are identified as solitons as predicted by the IST solutions (Kaup et al., 1979). They are consistent with the Manley Rowe relations which predict an asymptotic state with $|a_2|/|a_3| \approx 1$ for pump depletion. On the other hand, the collisional interaction exhibits nonsymmetric pulses with $a_3 \gg a_2$, which suggests a rather

By choosing the pump and sideband field polarizations as $E_{1,2} = E_{1,2}\,\hat{y}$, we see from the left hand side of (A.2) and (A.3) the associated linear density and temperature perturbations vanish (in the $(x,z)$ geometry), i.e.,

$$n^L_{1,2} = T^L_{1,2} = 0 \qquad \text{(A5)}$$

since the high-frequency waves are electromagnetic. For the low- frequency wave, the magnetized, cold, linear response as given by the left hand sides of (A1) - (A.3) is

$$v^L_3 = \frac{i\omega_3 \epsilon^e_3 \cdot E_3}{4\pi e n_o} \qquad \text{(A6)}$$

$$n^L_3 = \frac{n_o k_3 \cdot v^L_3}{\omega_3} \qquad \text{(A7)}$$

$$T^L_3 = \frac{2}{3}\,\frac{T_o k_3 \cdot v^L_3}{(\omega + i\Delta\nu)} \quad , \qquad \text{(A8)}$$

where $\epsilon^e_3$ is the electron contribution to the cold plasma dielectric tensor.

At the next order, we evaluate the thermal and nonlinear terms on the right hand sides of (A1)-(A.3), using the lowest-order solutions, (A.4)-(A.8). It can easily be seen that there is no nonlinear modification to the density at all three frequencies (i.e. right hand sides of (A2) vanishes),

## APPENDIX

The plane wave perturbations in a resonant three wave interaction satifsy the fluid equations (8)-(10) as follows

$$v + \frac{i}{(\omega+i\nu)}\frac{e}{m_e}\left[E + \frac{v \times B_o}{c}\right] = \frac{k}{(\omega+i\nu)}\frac{T_o}{m_e}\left[\frac{T}{T_o} + \frac{n}{n_o}\right]$$

$$- \frac{i}{(\omega+i\nu)}\left[v \cdot \nabla v + \frac{e}{m_e}\frac{vXB}{c} + \frac{T_o}{m_e}\left[\frac{T}{T_o} - \frac{n}{n_o}\right]\frac{\nabla n}{n_o}\right]_{\omega,k} \quad (A1)$$

$$n - \frac{n_o k.v}{\omega} = \frac{-i[\nabla \cdot nv]}{\omega} \quad \omega,k \quad (A2)$$

$$T - \frac{2}{3}\frac{T_o\ k.v}{(\omega+i\Delta\nu)} = \frac{-i}{(\omega+i\Delta\nu)}\left[v \cdot \nabla T - \frac{2}{3}(\nu m_e v - T\nabla) \cdot v\right]_{\omega,k} \quad (A3)$$

The subscripts $\omega$, k for the square brackets indicate that the appropriate convolution product of the other two waves is taken to meet the matching conditions of (11). Equations (A.1)-(A.3) can be solved perturbatively.

Our main interest concerns the decay of a high-frequency electromagnetic pump-wave ($\omega_1$, $k_1$) into a high-frequency sideband ($\omega_2$, $k_2$) and a low frequency mode ($\omega_3$, $k_3$) in the collisional regime. If we assume that the pump wave and its sideband have frequencies $\omega_{1,2} >> \omega_{ce}$, the electrons are unmagnetized, and the left hand side of (A) yields, to lowest order, their driven velocities in the linear, cold limit

$$v^L_{1,2} = \frac{-ieE_{1,2}}{m_e\omega_{1,2}}\left[1 - i\frac{\nu}{\omega_{1,2}}\right] \quad (A4)$$

## ACKNOWLEDGEMENTS

The authors wish to thank C. L. Chang, A. T. Drobot, and S. Ossakow for many helpful discussions. This work was supported by the U.S. Naval Research Laboratory contract N00014-82-M-0133.

The Editor thanks the two referees for their assistance in evaluating this paper.

electron heating will be required to support proper experimental effort. Meanwhile the paper should be used as a guide to the physics expected during the interaction and the approximate design of ionospheric heaters required for a proof of principle experiment.

Before closing we should note that S. Ganguly and W. Gordon (1984) reported preliminary evidence for beat wave generation for frequencies between 10 and 40 Hz, using the Arecibo HF facility. Their results were consistent with power threshold scaling increasing linearly with $f_3$. The preliminary nature of the experimental results and the fact that the interaction region was in the $F$ rather than the $E$ region, where heat conditions, neglected in our analysis, dominate the energy transport, does not allow for a quantitative comparison of our theory with the experiment.

## 5. SUMMARY AND CONCLUSIONS

We have examined stimulated excitation of ELF waves in the lower ionosphere by the use of two HF pumps. Previous work [*Papadopoulos et al.*, 1982, 1983] addressed the excitation of Alfven and magnetosonic modes by similar techniques. However, since for ionospheric conditions $\nu_3 \geq \omega_{ci}$ up to 150 km, excitation of these modes is possible only above that height. The thermal ponderomotive force driving the interaction is proportional to the electron-neutral collision frequency $\nu$ which is by more than two orders of magnitude smaller above 150 km than near 100 km. The discovery that the helicon mode [*Menyuk and Papadopoulos*, 1984) is a proper eigenmode of the system even for frequencies with $\omega_3 < \nu_3$ allowed us to reduce the threshold for excitation of ELF waves below 100 Hz by more than two orders of magnitude, by coupling to the helicon mode in the vicinity of 100 km altitude. In addition to focusing on the helicon mode, a more detailed description was presented of the parametric decay processes in dissipative media discussed previously in a letter [*Papadopoulos et al.*, 1983]. As noted, a more comprehensive analysis including the effects of oblique propagation of the pump from the ground to the ionosphere, the inhomogeneous structure of the pump in the interaction region, the inhomogeneous structure of the ionosphere, and a self-consistent description of the

from (50), by taking $k_{2x}/k_{3x} \approx .5$, $T_e \approx 10^3$ °K, and $\omega_1/\omega_{pe} \approx 2$. The value of $\omega_1/\omega_{pe} \approx 2$ implies a 30° incidence angle of the transmitter, which is sufficient to achieve long propagation paths (*Ginzburg*, 1970). Using these values (50) becomes

$$P_{THR} = 62 \left[\frac{10^5}{n_o}\right] \left[\frac{10^{12}}{N}\right] \left[\frac{f_3}{100\ Hz}\right] \quad MW \qquad (51)$$

Table *1* shows the power required to excite 100-Hz and 50-Hz waves as a function of height as computed by (51). The last column shows the required pump frequency versus height based on 30° incidence. Daytime conditions were assumed in compiling Table *1* (*Gurevich*, 1978). Notice that the optimum interaction height is 100-km, and relatively modest power is required. We would like to stress that the values in Table *1* are indicative rather than exact. We feel that the assumption of $T_e \approx 10^3$ °K is very conservative and $T_e \approx 3\text{-}4 \times 10^3$ °K is more realistic. This will reduce the power requirement by factors of 3 - 4. On the other hand a variety of propagation losses have been neglected. These will be considered in the future. It is interesting to note that $P_{THR} \sim (1/n_o)\ (1/N)$. Therefore further reduction in $P_{THR}$ can be achieved if we could increase the local ionization by long pulse radiation previous to the beat excitation.

we note that the ion neutral collision frequency $\nu_3 > \omega_{ci} \approx 220\ s^{-1}$ for altitudes below 130 km, which is the region of interest in the present work. Therefore to excite low-frequency waves below 100 Hz, we must couple nonlinearly to the newly discovered helicon branch given by Eqs. (7). As discussed in Section 2, this branch occupies the range $\omega_3 < \nu_3$ and extends to very low frequencies. It is important to notice that contrary to the conventional situation, where the currents associated with the low-frequency waves are carried by the ions, in the helicon branch the currents are carried by the electrons. The ion dynamics is viscously frozen due to the high collisionality ($\nu_3 > \omega_{ci}$). Under these circumstances the Alfven and magnetosonic modes are not proper eigenmodes.

Figure 5 is a schematic of the geometry in which two HF waves ($\omega_1$, $k_1$), ($\omega_2$, $k_2$) interact nonlinearly in the ionosphere to drive a helicon with $\omega_3 < \nu_3$. The HF pump is incident at a small angle to $B_0$ with a beam width equal to or smaller than the local density scalelength $L_n$. For $\omega_1$, $\omega_2 >> \omega_3$ the resonance conditions (11) yield a $k_3$ that propagates almost directly downward. Such an interaction configuration can be achieved by grazing incidence of the HF beams at the desired ionospheric height (Figure 6).

Approximate values of the required power can be found

$$\cdot \left[\frac{10^{3}\,^{\circ}K}{T_e}\right] \left[\frac{f_3}{100\ Hz}\right] \ MW \ . \qquad (50)$$

The threshold power scales linearly with frequency, so that it is smaller for the lowest frequencies for which the analysis is applicable. The optimum interaction region height can be found by maximizing the product $n_o N$. This is due to the weak dependence of the terms $(\omega_1/\omega_{pe})$ and $(k_{2x}/k_{3x})$ on the exact plasma parameters. We will further elaborate on these later on.

We proceed next to use the above equations in the design of a proof of principle ionospheric heating experiment. For convenience our estimates refer to the case where the magnetic field is perpendicular to the density gradient (Figure 5). This might not be the optimal case. Determination of the optimal geometry requires generalization of our calculation to include the effects of pump propagation between the ground and the interaction region, and the inhomogeneous structure of the pump near the reflection surface. These issues are currently under study and will be reported elsewhere. Before comparing the threshold conditions for the nonlinear interaction we examine the type of low-frequency waves of interest for our particular application. The dispersion relation for the low-frequency ionospheric modes was discussed in Section 2. Referring to typical ionospheric conditions (Gurevich, 1978)

and substituting for $\beta$ explicitly, we obtain

$$|E_1(z=0)| = \frac{4mc^2}{e} \frac{\omega_1 \omega_{ce}}{\omega_{pe}^2} \left|\frac{k_{2x}}{k_{3x}}\right| \left[\frac{L}{\tilde{\ell}_c}\right] \frac{1}{|\Lambda|^{1/2} L} \qquad (46)$$

The requirement for absolute instability leading to complete decay is given by (42b). Therefore the threshold electric field found from (46) by taking $L/\tilde{\ell}_c \approx 2$ is

$$|E_1(z=0)|_{THR} = 4 \times 10^2 \left[\frac{10km}{L}\right] \left[\frac{\omega_1 \omega_{ce}}{\omega_{pe}^2}\right] \left|\frac{k_{2x}}{k_{3x}}\right| \frac{1}{|\Lambda|^{1/2}} \frac{V}{m} \qquad (47)$$

For ionospheric conditions $\omega_{ce} = 7.5 \times 10^{6\ -1}$ and $\nu = 2.5 \times 10^{-11}\ N\ Te^{\ -1}$ based on ion neutral collisions; $N$ is in $cm^{-3}$ and $T_e$ in $^\circ K$. Using these values (47) can be written in practical units as

$$|E_1(z=0)|_{THR} = 22 \left[\frac{\omega_1}{\omega_{pe}}\right] \left|\frac{k_{2x}}{k_{3x}}\right| \left[\frac{10\ km}{L}\right]$$

$$* \left[\frac{10^5 cm^{-3}}{n_o}\right]^{1/2} \left[\frac{10^{12} cm^{-3}}{N}\right]^{1/2} \left[\frac{10^3 {}^\circ K}{T_e}\right]^{1/2} \left[\frac{f_3}{100\ Hz}\right]^{1/2} \frac{V}{m} \qquad (48)$$

The power required to achieve this can be found from (47) by assuming that the HF illluminated region is a square with side $L$. Then

$$P_{THR} = \frac{1}{2} \epsilon_0\ c\ |E_1(z=0)|^2_{THR} \qquad (49)$$

Notice that the resulting equation is independent of $L$. From (48) and (49) we find that in practical units

$$P_{THR} = 64 \left[\frac{\omega_1}{\omega_{pe}}\right]^2 \left[\frac{k_{2x}}{k_{3x}}\right]^2 \left[\frac{10^5\ cm^{-3}}{n_o}\right] \left[\frac{10^{12}\ cm^{-3}}{N}\right]$$

case apply to the steady state interaction as well. Rather than energy, here one looks at the downconversion of HF power into the ELF/VLF signal. In analogy with (41), we can write the power downconversion efficiency out to a distance $z$ as

$$\frac{P_3(z)}{P_1(0)} = \frac{\omega_3}{\omega_1} \frac{\int_{-\infty}^{\infty} dx \left[ |\tilde{a}_1(0)|^2 - |\tilde{a}_1(z)|^2 + \frac{\nu}{\omega_3} \sigma(z) \right]}{\int_{-\infty}^{\infty} dx |\tilde{a}_1(0)|^2} , \quad (43a)$$

where

$$P_j = \omega_j |\tilde{a}_j|^2 , \quad (43b)$$

$$\sigma(z) = \frac{8}{3} |\tilde{K}| \int_0^z dz \; Re \; (\tilde{a}_1^* \; \tilde{a}_2 \; \tilde{a}_3) \quad (43c)$$

Therefore, in the collisional limit, the amount of ELF power one can generate may exceed the collisionless maximum $\omega_3/\omega_1$ set by the Manley-Rowe relations, even when total pump depletion does not take place.

Of great practical interest to the ELF generation is the pump requirement for absolute instability. From the definition of $\tilde{\ell}_c$, we can solve for the incident pump field

$$|E_1(z=0)| = \frac{\omega_1}{|\beta|} \left| \frac{\partial D_2}{\partial k_{2x}} \; \frac{\partial D_3}{\partial k_{3x}} \right| \frac{1}{|\Lambda|^{\frac{1}{2}} \tilde{\ell}_c} , \quad (44)$$

where we have used (25) and (27) for $\tilde{v}_2$, $\tilde{v}_3$, $k$, and $\tilde{a}_1$ in (42c). Recognizing

$$\frac{\partial D_j}{\partial k_{jx}} = -2k_{jx} \quad (45)$$

## IV STEADY-STATE INTERACTION-ELF GENERATION

Relevant to the ELF generation scheme is the steady state interaction given by (26). With the time variable replaced by z, the initial value problem we hitherto considered turns into a boundary value problem. The absolute instability found previously, which corresponds to an oscillator in time, now describes an amplifier in space for the low-frequency wave. In the nonlinear saturation stage, the pump depletes as it propagates. Due to the fact that (24) and (26) are equivalent systems, it is straightforward to see that the conditions for absolute instability in the steady state case are

$$\tilde{v}_2\tilde{v}_3 < 0 \tag{42a}$$

and

$$L > 1.8\ \tilde{\ell}_c \tag{42b}$$

where

$$\tilde{\ell}_c = \frac{|\tilde{v}_2\tilde{v}_3|^{\frac{1}{2}}}{|\tilde{K}^*\tilde{a}_1\ (z=0)|\,|\Lambda|^{\frac{1}{2}}} \tag{42c}$$

Since $v_{2z}, v_{3z} > 0$, (42a) coincides with (28a) while (41b) can be shown to be identical to (37), i.e. $\tilde{\ell}_c = \ell_c$, if one replaces the initial condition $a_1$ (t=0) in $\ell_c$ by the boundary condition $a_1$ (z=0). It follows that the conclusions of the nonlinear analysis on the time dependent

$$\frac{3(t)}{1(0)} = \frac{\omega_3}{\omega_1} \left[ \frac{\int_{-\infty}^{\infty} dx \left[ |a_1(0)|^2 - |a_1(t)|^2 + \frac{\nu}{\omega_3} \sigma \right]}{\int_{-\infty}^{\infty} dx \, |a_1(0)|^2} \right] \qquad (41)$$

It is easy to see that in the collisionless limit, the maximum downconversion efficiency one can achieve is $\omega_3/\omega_1$ if the pump is completely depleted, i.e., $a_1(t) = 0$. In the example we consider, $a_1(t) \neq 0$ so that the downconversion efficiency is less than $\omega_3/\omega_1$. The collisionless maximum $\omega_3/\omega_1$, a consequence of the Manley-Rowe relations, can be exceeded in the collisional interaction when the collisional heating term dominates the pump depletion term, $|a_1(t)|^2$. Due to the large factor $\nu/\omega_3$, this may occur when the three waves overlap even over a short duration. As Figure 4 shows, the downconversion efficiency indeed exceeds $\omega_3/\omega_1$ without total depletion of the pump. Therefore, we have the new interesting result that in a collisional interaction, the Manley-Rowe relations no longer set the limit for the downconversion efficiency. The determining factor in this case is the cumulative collisional heating over time. The effect is most significant when the convection of the decay waves out of the pump is slow so that $\sigma$ has the largest integrated value possible. Under such conditions, the downconversion efficiency exceeds the collisionless maximum $\omega_3/\omega_1$.

the Manley-Rowe relations predict, the collisionless interaction yields a value equal to the frequency ratio $\omega_3/\omega_2 = 0.01$.

The present numerical results can be shown to be consistent with the action relations we previously derived. Subtracting (38a) from (38*b*) and integrating in time, we obtain ($\Gamma_j = 0$)

$$\int_{-\infty}^{\infty} dx \; (|a_3(t)|^2 - |a_2(t)|^2) = \frac{\nu}{\omega_3} \int_{-\infty}^{\infty} dx \; \sigma \qquad (40a)$$

where

$$\sigma = \frac{8}{3} |K| \int_0^t dt \; Re \; (a_1^* \; a_2 \; a_3) \qquad (41b)$$

For the collisionless interaction ($\nu = 0$), (40a) simply states that the transfer of action to $a_2$ and $a_3$ are identical; hence the appearance of symmetric pulses in Figure 2. It then follows directly that the energy ratio in Figure 4 should be equal to $\omega_3/\omega_2$, which it is. In the collisional case, (40a) implies a net gain in action-transfer to $a_3$, and we observe numerical evidence to this in the emergence of nonsymmetric pulses as well as in the increase in $_3(t)/\ _2(t)$. An expression for the down-conversion efficiency may be obtained from (38*b*) by an integration in time ($\Gamma_j = 0$)

different action transfer picture than that described by the Manley-Rowe relations. We have plotted in Figure 3, the percentage change of $c_{12}$ and $c_{13}$ with time. While there is a moderate decrease in $c_{12}$, the increase in $c_{13}$ is dramatic. The preferential transfer of action to $a_3$ is understandable in view of the large factor $\nu/\omega_3$ in the low frequency equation as compared to the small correction $\nu/\omega_1$ in the equation for $a_2$. Physically, the enhancement is due to additional $\omega_3$ photons that are being generated at a large rate via the temperature perturbation as a result of electron heating by the high-frequency waves. This is achieved at the expense of the total energy $\gamma$ which suffers a net loss to the medium as evident by the long-time decrease shown in Figure 3. In comparison, the corresponding collisionless interaction displays no noticeable change in any of the three quantities considered.

Of particular interest to the ELF/VLF generation is the efficiency with which one can downconvert the pump power into the low-frequency wave $\omega_3$. Toward this end, we have calculated the downconversion efficiency $_3(t)/\ _1(0)$ for both the collisional and collisionless interaction. Figure 4 shows an order-of-magnitude (~20) enhancement of the former over the latter. Also shown is the energy ratio $_3(t)/\ _2(t)$. Again we find that the collisonal interaction assumes a much larger value (~0.8) at pump depletion. As

$$n_j^{NL} = 0 \quad j = 1,2,3 \tag{A9}$$

whereas the nonlinear temperature perturbation is due only to Ohmic heating,

$$T_j^{NL} = i\frac{2}{3}\frac{e}{(\omega_j + i\Delta\nu)} \left[\nu m_e v^2\right]_{\omega_j, k_j} \tag{A10}$$

Since the thermal pressure does not affect the electron velocities at high frequencies ($T^L_{1,2} = 0$) we find using (A1) the nonlinearly perturbed velocities

$$v^{NL}_{1,2} = \frac{-ieE^{NL}_{1,2}}{m_e(\omega_{1,2} + i\nu)} \tag{A11}$$

where

$$E^{NL}_{1,2} = \frac{ik_{1,2}T^{NL}_{1,2}}{e} + \left[\frac{m_e v^L \cdot \nabla v^L}{e} + \frac{v^L \times B}{c}\right]_{\omega_{1,2}, k_{1,2}}$$

$$= E^T_{1,2} + E^P_{1,2}. \tag{A12}$$

To arrive at (A.11), we have combined the terms on the right hand side of (A.1) with the electric field term on the left hand side and defined the nonlinear fields $E^{NL}_{1,2}$ which contain, in addition to the Ohmic heating $E^T_{1,2}$, the ponderomotive contributions within the square brackets, $E^P_{1,2}$. In a similar fashon, the nonlinearly perturbed velocity at low frequency is given by

$$v^{NL}_3 = \frac{i\omega_3 \epsilon^e_3 \cdot E^{NL}_3}{4\pi e n_o} \tag{A13}$$

where

$$E_3^{NL} = \frac{ik_3 T_3^{NL}}{e} + \left[\frac{v^L XB}{c}\right]_{\omega_3, k_3} \equiv E_3^T + E_3^P \qquad (A14)$$

Here, the ponderomotive field is entirely due to the E X B drift of electrons. For our parameters of interest, the linear thermal pressure $n_o^L T_3$ turns out to be neglisible and has been ignored.

The nonlinear current densities that drive the high frequency waves $\omega_1$, $\omega_2$ are due to the nonlinearly perturbed velocities $v^L_{1,2}$ and to the beating of the linear velocities $v^L_{1,2}$ with the low-requency density perturbation $N^L_3$,

$$\begin{aligned} J_1^{NL} &= -e\left[n_o v_1^{NL} + n_3^L v_2^L\right] \\ J_2^{NL} &= -e\left[n_o v_2^{NL} + n_3^{L*} v_1^L\right] \end{aligned} \qquad (A15)$$

where the asterisk superscript denotes the complex conjugate. We keep only the second of the two contributions to $J^{NL}_{1,2}$ since it can be shown that its effect is greater by the ratio of high-frequency to low-frequency phase velocities. Expressing $nL_3$, $v^L_{1,2}$ explicitly in terms of the electric fields via equations (A.4), (A.6) and (A.7), (A.15) become

$$\begin{aligned} J_1^{NL} &= \frac{-e}{4\pi m_e}\frac{E_2}{\omega_2}\left[1 - \frac{i\nu}{\omega_2}\right]\left[k_3 \cdot \epsilon_3^e \cdot E_3\right] \\ J_2^{NL} &= \frac{e}{4\pi m_e}\frac{E_1}{\omega_1}\left[1 - \frac{i\nu}{\omega_1}\right]\left[k_3 \cdot \epsilon_3^e \cdot E_3\right]^* \end{aligned} \qquad (A16)$$

The low-frequency nonlinear current density, however, is caused solely by the nonlinearly perturbed velocity, i.e.

$$J_3^{NL} = -en_o v_3^{NL} \tag{A17}$$

because all high frequency density perturbations vanish. The two nonlinear fields that drive $\Phi^{NL}_3$ are evaluated separately. Substituting (A.10) for $T^{NL}_3$, we have for the thermal field

$$E_3^T = \frac{4}{3}\, \nu m_e \frac{k_3}{\omega_3}\; v_1^L \cdot v_2^{L*} \tag{A18}$$

where $\Delta\nu$ has been neglected when compared to $\omega_3$. If one replaces $\Phi^L_{1,2}$ by (A.4), applies the frequency matching condition and assumes $\omega_1 \sim \omega_2$, $E_3^T$ may be further reduced to

$$E_3^T = -\frac{4}{3}\frac{e}{m_e}\frac{(E_1 \cdot E_2^*)}{\omega_1\omega_2}\; k_3 \frac{\nu}{\omega_3} \tag{A19}$$

Similar treatment on the ponderomotive field

$$E_3^P = \frac{v_1^L \times B_2^* + v_2^{L*} \times B_1}{c} \tag{A20}$$

yields

$$E_3^P = \frac{ie}{m_e}\frac{(E_1 E_2^*)}{\omega_1\omega_2}\left(k_3 + \frac{i2\nu}{\omega_1} k_1\right) \tag{A21}$$

where we have related $B_{1,2}$ to $E_{1,2}$ via Faraday's law and have made simplifications using vector identities. Dropping the contribution proportional to $k_1$ because it is smaller compared to $k_3$, we finally obtain

$$J_3^{NL} = \frac{e}{4\pi m_e} \frac{\omega_3}{\omega_1 \omega_2} \epsilon_3^e \cdot k_3 \left[E_1 \cdot E_2^*\right]\left[1 + i\frac{4}{3}\frac{\nu}{\omega_3}\right] \qquad (A22)$$

It is clear from (A.22) that the thermal nonlinearity dominates when $\nu/\omega_3 \gg 1$, introducing an equivalent enhancement factor as well as a $\pi/2$ phase difference.

Fig. 1a.— Real part of $\eta\ell_c$ ($\eta L_c$) versus $L/\ell_c$ ($L/L_c$) for the collisional (collisionless) interaction. The dotted lines refer to the collisionless case.

Fig. 1b. Imaginary part of $\eta\ell_c$ ($\eta L_c$) versus $L/\ell_c$ ($L/L_c$) for the collisional (collisionless) interaction. The dotted line at zero is for the collisionless case.

Fig. 2. Waves profiles at t=25.0 for the collisional (solid lines) abnd collisionless (dotted lines) interactions.

Fig. 3. Percentage change in the sums of the actions $c_{12}$, $c_{13}$ and the total energy $T$ versus time. The dotted line indicates zero change for the collisionless interaction.

Fig. 4. The energe ratio $\epsilon_3(t)/\epsilon_2(t)$ and the down-conversion efficiency $\epsilon_3(t)/\epsilon_1(0)$ versus time for the collisional (solid lines) and collisionless (dotted lines) interactions.

Fig. 5. Geometry of three-wave interaction in the lower ionosphere.

Fig. 6. Schematic of practical ELF generation scheme by grazing incidence of two HF heaters in the ionosphere.

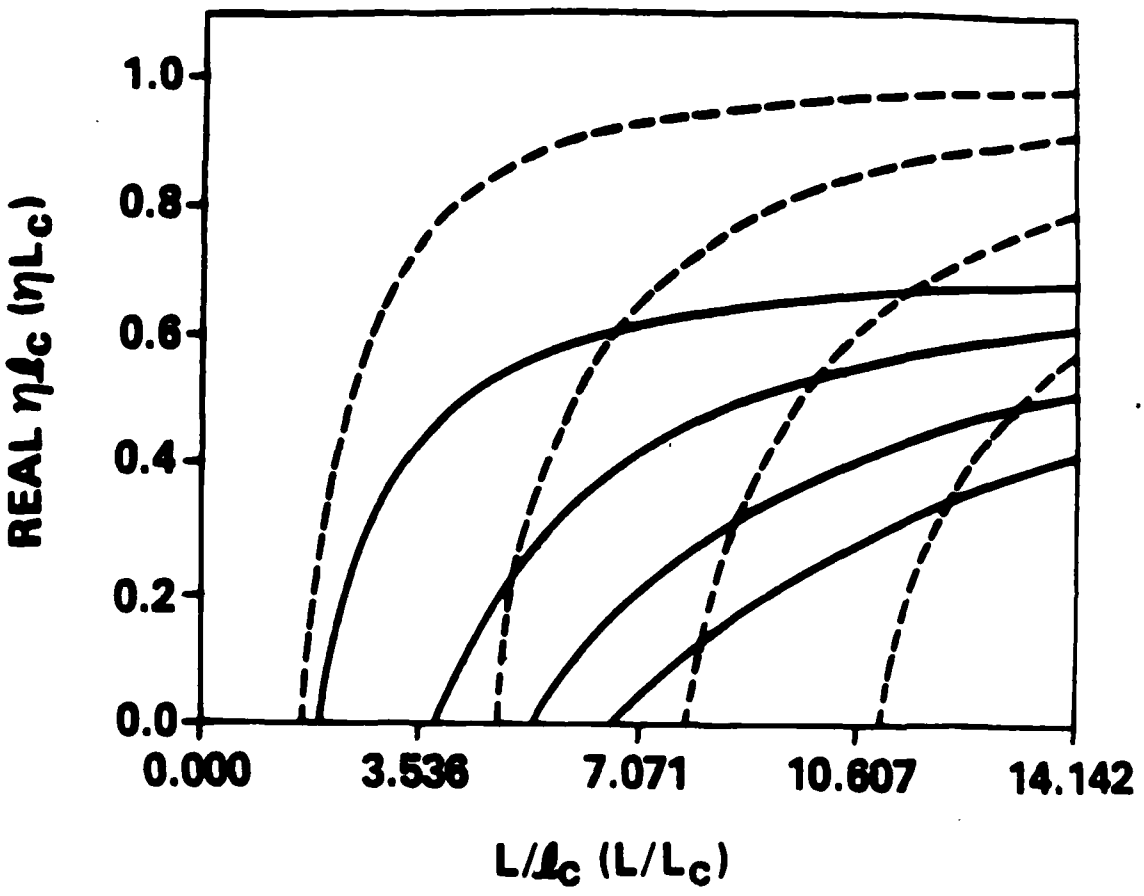
1.0
0.8
0.6
0.4
0.2
0.0
REAL ηLc (ηLc)
0.000
3.536
7.071
10.607
14.142
L/Lc (L/Lc)

**FIGURE 1a.**

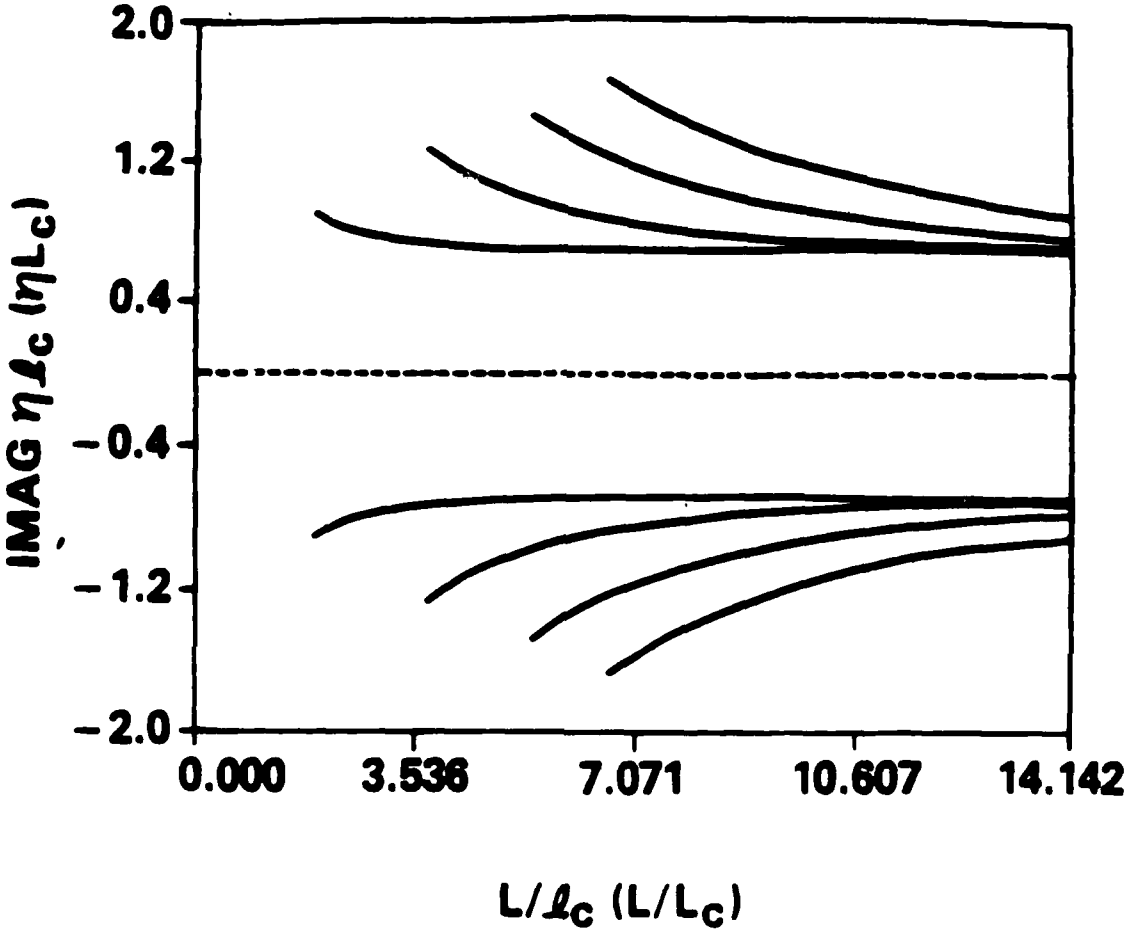
2.0
1.2
0.4
-0.4
-1.2
-2.0
IMAG ηLc (ηLc)
0.000
3.536
7.071
10.607
14.142
L/ℓc (L/Lc)

FIGURE 1b.

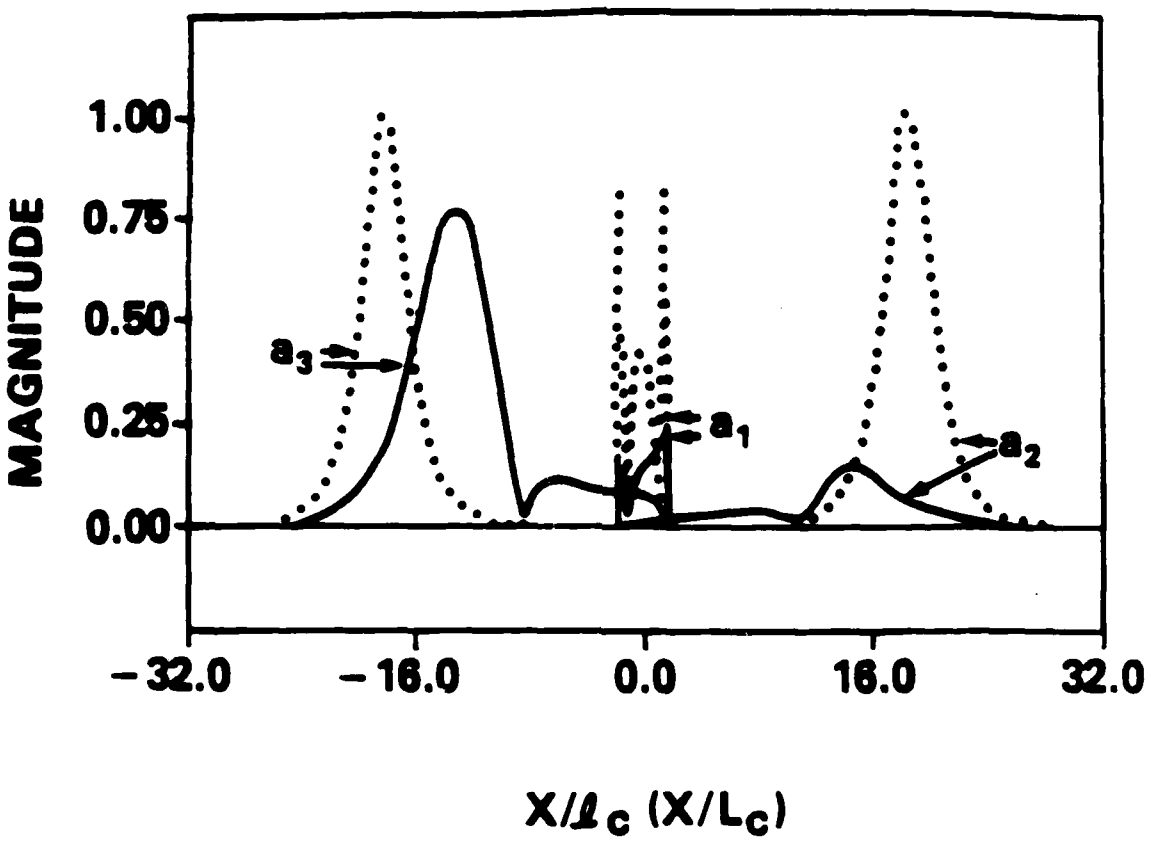
MAGNITUDE
1.00
0.75
0.50
0.25
0.00
$a_3$
$a_1$
$a_2$
-32.0
-16.0
0.0
16.0
32.0
$X/\ell_c$ ($X/L_c$)

**FIGURE 2.**

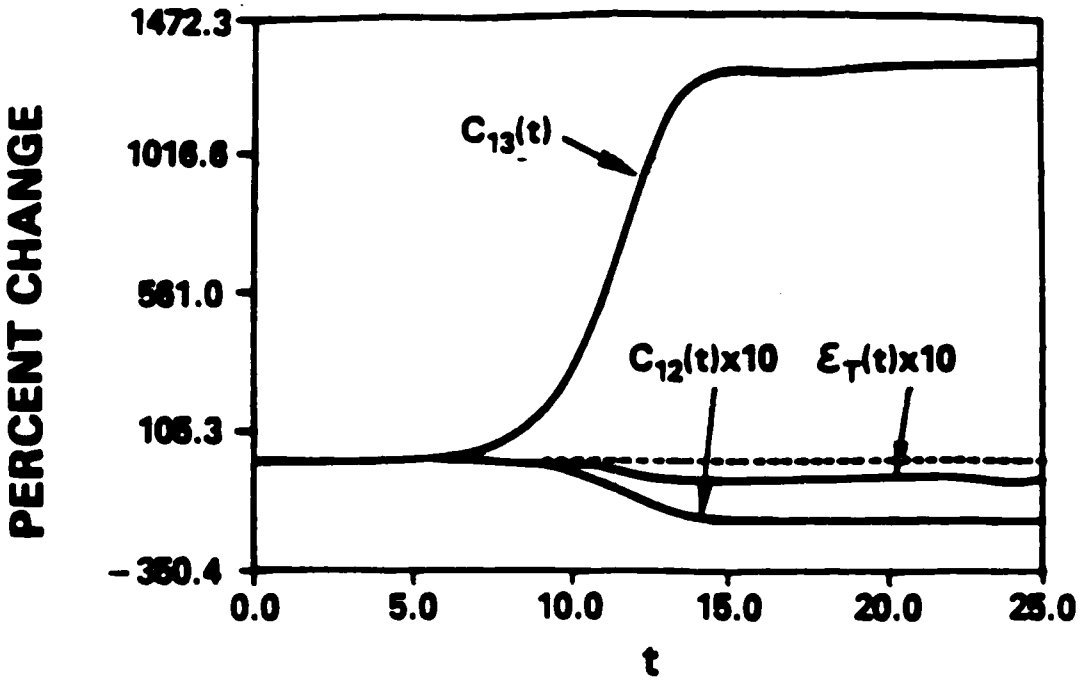
1472.3
1016.6
561.0
106.3
-350.4
PERCENT CHANGE
$C_{13}(t)$
$C_{12}(t)x10$
$\varepsilon_T(t)x10$
0.0
5.0
10.0
15.0
20.0
25.0
t

**FIGURE 3.**

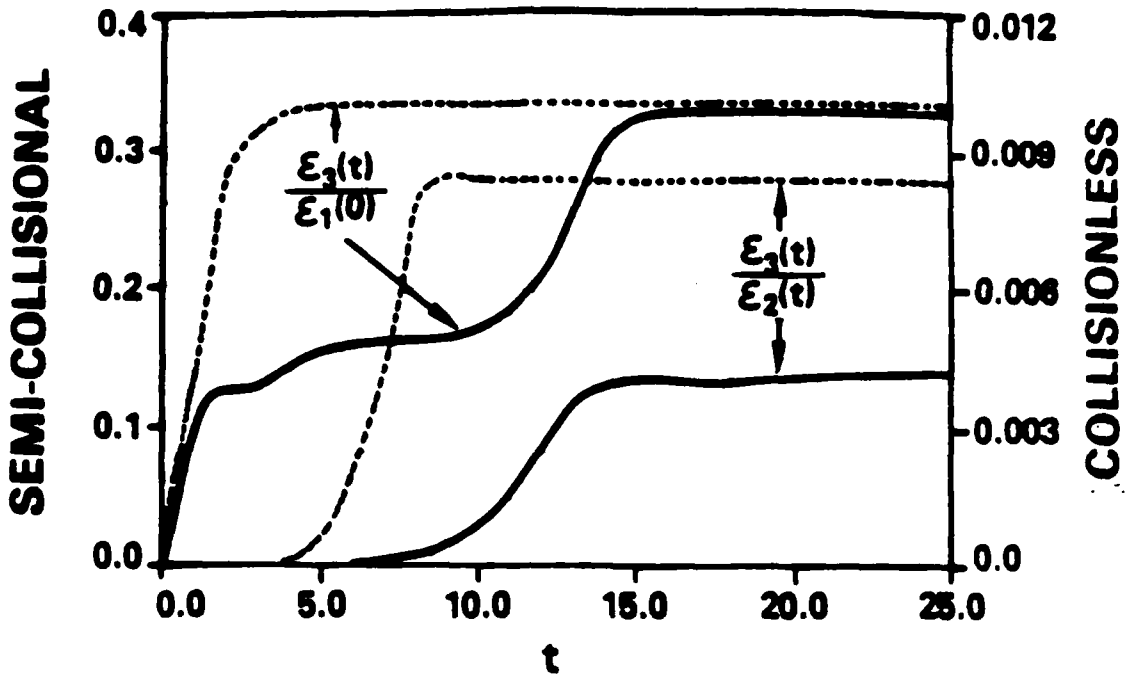
SEMI-COLLISIONAL
COLLISIONLESS
0.4
0.3
0.2
0.1
0.0
0.012
0.009
0.006
0.003
0.0
0.0
5.0
10.0
15.0
20.0
25.0
t
$\frac{\varepsilon_2(t)}{\varepsilon_1(0)}$
$\frac{\varepsilon_2(t)}{\varepsilon_2(t)}$

**FIGURE 4.**

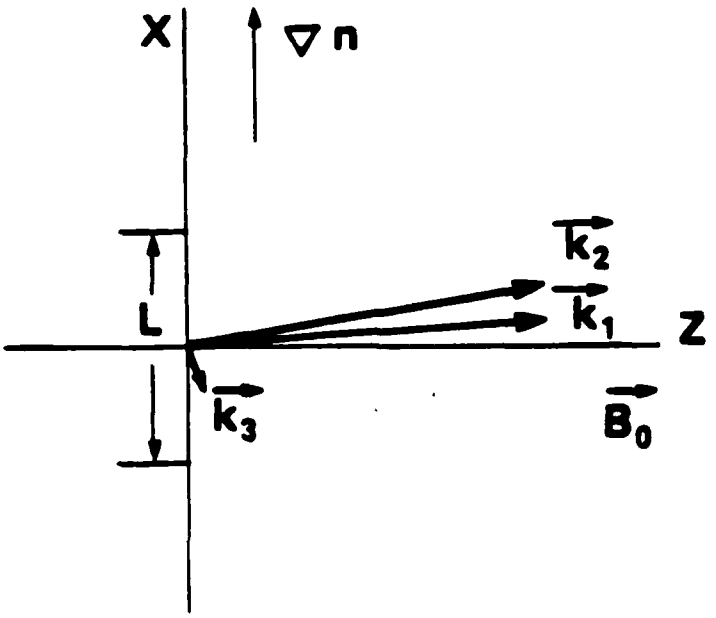


**FIGURE 5.**

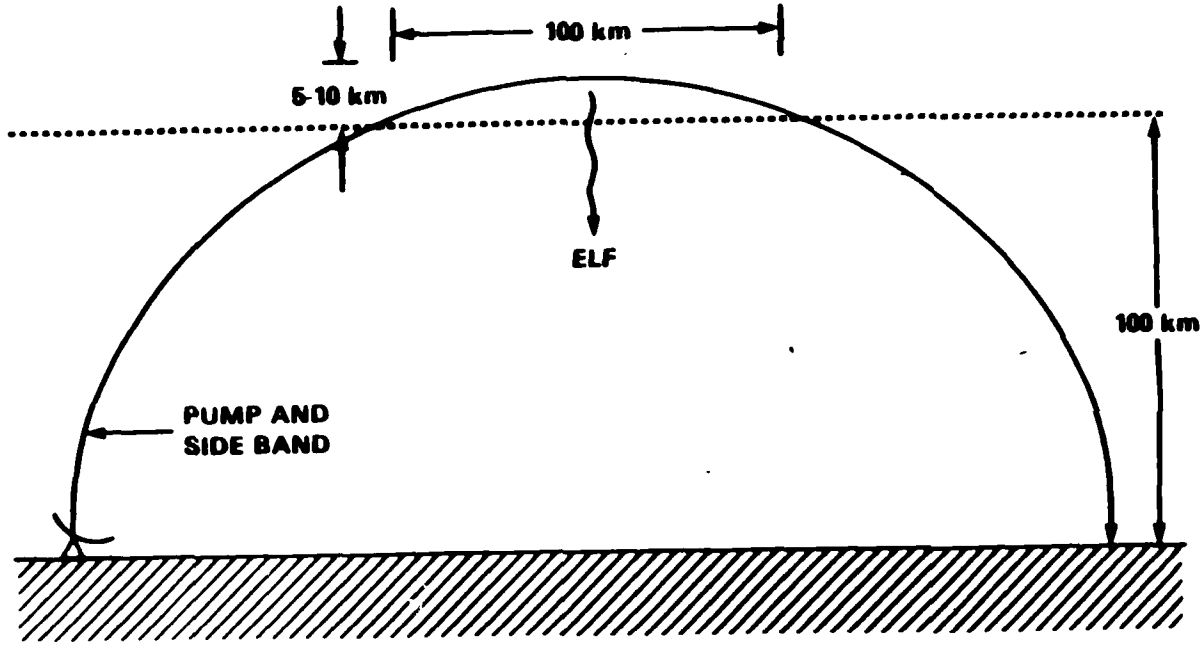


**FIGURE 6**

TABLE 1

| Height | $P_{THR}^{MW}$ 100 Hz | $P_{THR}^{MW}$ 50 Hz | 25 Hz | $f_1$ MHz |
|---|---|---|---|---|
| 90 | 15 | 7.5 | 3.75 | 2.5 |
| 100 | 8 | 4 | 2 | 5 |
| 110 | 26 | 13 | 6.5 | 6 |
| 120 | 60 | 30 | 15 | 6.4 |

Threshold Power for Excitation of 100, 50, and 25-Hz Waves versus Ionospheric Heights. The last column gives the required pump frequency (based on equation (51).

dominance of the EW magnetic component. First, the absence of a vertical field component implies that the nonlinear current flows horizontally in the ionosphere in a rather thin sheet. From Ref. 4 we note that $\underline{J}^{NL}_3 \sim \epsilon^3 \cdot \underline{k}_3$ where $\epsilon^3$ is the low frequency dielectric tensor. Since the dominant element of $\epsilon^3$ is the off diagonal ($\epsilon^3_{xy}$) the current flows on a plane perpendicular to $\underline{k}_3$ and for wavepacket interactions in the horizontal direction will produce no vertical field. The predominance of the EW component over the NS is consistent with the interaction occurring predominantly in NS direction which is the direction of the magnetic meridian plane. Notice that in the F-region, where the field aligned Pederson conductivity is dominant, most of the currents are forced to flow in the N-S direction. If the interactions would have occurred in the E-region, where the Hall conductivity prevails, we would have expected a different polarization for the ULF signal. Finally, the unsteady nature of the signals could be either due to: (i) We were operating very near threshold, which was attained only for certain ionospheric conditions or (ii) Nonlinear self modulation or dissipation effects forced the system to behave like a quenched oscillator. Which is the case will require further experimentation and better diagnostics.

The concept tested on the second set of experiments was similar to the spontaneous magnetic field generation in

$$B_3 = 320\ \eta^{\frac{1}{2}} \left[ \frac{P_1}{200kw} \right]^{\frac{1}{2}} \left[ \frac{50km}{R} \right] m\gamma \qquad (2)$$

where R is the beam radius in the F region and $\eta$ is given by

$$\eta_C = \frac{\omega_3}{\omega_1} \qquad (3a)$$

in the collisionless region ($\nu \ll \omega_3$) and

$$\eta_S = \left[ \frac{\omega_3}{\omega_1} \right] \left[ \frac{\nu}{\omega_3} \right] \qquad (3b)$$

in the semicollisional regime ($\nu > \omega_3$). For our parameters $\eta_C = 10^{-6}$ and $\eta_S = 3x10^{-5}$. Eq. (2) with $\eta_C = 10^{-6}$ gives .32 $m\gamma$ which is smaller than the observed. For $\eta_S = 3x10^{-5}$, we find $B_3 \sim 1.7\ m\gamma$. On the basis of the above admittedly crude estimates, we can conclude that the signals produced exceed the upper maximum expected from Manley Rowe relations and are in line with the predictions of the dissipative three way coupling[2,3].

The absence of informations concerning the precise coupling geometry and the direction of the density gradients, makes difficult any quantitative comparison with observations relying on the flow pattern of the nonlinear currents. We can only comment on the implications of the

where $\omega_e$, $\Omega_e$ are the plasma and cyclotron frequency, L is the pump width and $\Lambda = 1 + i\ 4/3\ \nu/\omega_3$ where $\nu$ is the dominant electron collision frequency. For $\omega_3 \ll \nu$, and $k_2x/k_3x \approx .5$ we find

$$E_{THR} = \left[\frac{10km}{L}\right]\left[\frac{\omega_1}{\omega_e}\right]\left[\frac{\Omega_e}{\omega_e}\right]\left[\frac{f_3}{\nu}\right]^{1/2}\frac{V}{m} \qquad (1b)$$

For the case under consideration the interaction occurs in the F-region rather than the E-region considered in Refs. 2,3. Therefore, $\nu$ corresponds to the electron-ion collision frequency, which we take as $10^3$, $\Omega_e/\omega_e \approx 1/3$ and L ≈ 60km of the order of the density gradient. We also take the ratio $\omega_1/\omega_e \approx 1/\sin\theta \approx 2$ by using an upper limit of $\theta \approx 30°$, the HF beam cone. With these values we find $E_{THR} \approx 2\text{-}3$ V/m. For the Arecibo transmitter with 400 kw power and 22-25 db antenna gain the field in the F-peak region will be of the order of $E_F = .3\ \alpha$ V/m where $\alpha$ is the upswelling factor in the vicinity of the reflection area which is of the order 5-10. Therefore the Arecibo transmitter fields in the F-peak are of the order required for stimulated beat wave excitation for $f_3 <$ 5-10 Hz. On the basis of achieving maximum theoretical efficiency[4] the low frequency magnetic field will be given by

four transmitters were turned on/off at equivalent ULF rates of 5.0 and 6.25 Hz. There was good coincidence of the transmitter operation and ULF detection. An example of such generation for 5.0Hz signal is shown in Fig. 3. The duration of this experiment was too short to compile any meaningful statistics.

The limited number of experimental results as well as the absence of diagnostics of the modifications occurring in the ionosphere preclude at present anything but the most crude comparison of the results with the theoretical predictions. For the beat excitation the theoretical analysis considered the geometry shown in Fig. 4. Two HF pumps $(\omega_1, \underline{k}_1)$, $(\omega_2, \underline{k}_3)$ were interacting to generate a low frequency wave $(\omega_3, \underline{k}_3)$ satisfying the conditions $\omega_1-\omega_2 = \omega_3$. The analysis performed on the basis of wave-packet interactions predicts stimulated beat wave ecitation leading to pump depletion for HF threshold electric field in the interaction region given by[3]

$$E_{THR} = 4\times10^{2} \left[ \frac{10km}{L} \right] \left[ \frac{\omega_1 \Omega_e}{\omega_e^{2}} \right] \left[ \frac{k_{2x}}{k_{3x}} \right] \frac{1}{|\Lambda|^{\frac{1}{2}}} \frac{V}{m} \qquad (1)$$

and the Schumann resonance near 8 Hz. Fig. 1 shows an example of the data for HF operation at 5.1 MHz and (5.1 MHz + 5 or 3 Hz). The HF transmitters were operating at a difference of 5 Hz during 16.30-17.30 AST. The frequency difference was changed to 3 Hz at 17.30 AST and then back to 5 HZ at 18.00 AST. These data are shown as power spectra over the frequency 0-10 Hz in Fig. 1. The peaks correspond to absolute values of 150-350 $\mu\gamma/\sqrt{Hz}$ and a signal to noise ratio of about one. It is worth noting that there were no communications on Mona and the operators identified the 3 and 5 Hz signals without any prior knowledge except for the prearranged schedule that changes will be made every hour or half hour and the beat frequency will be between 0-10 Hz. All three components of the field were monitored during these experiments. Significantly though, the signals were received only in the coil aligned in the East/West direction, while there was no detectable signal in either the North/South or vertical component of the magnetic field. The coherent nature of the signal can be used to improve the S/N ratio by using narrower filter. A significant finding was that the signal had considerable fading. The fading determined the narrowest filtering. Using a 5mH filter the S/N ratio increased in occasional bursts as much as 50 with signal strength of the order of 1 $m\gamma/\sqrt{Hz}$. This is shown in Fig. 2 for the 3 and 5 Hz component.

In the second type of experiment (Feb. 12, 1985), all

The experiments were performed during the period Jan. 31-Feb. 15, 1985, using the Arecibo Observatory facilities. The HF transmitters were operated at 5.1 MHz and 3.1 MHz at a power of 4x100 kw which was fed into an antenna of 22-25 dB gain. The receiving system was built around sensors borrowed from the Engineering Geoscience Group, Dept. of Material Sciences, University of California, Berkeley. The low noise induction coils used[6] had a flat response for magnetic field in the frequency band .001-500 Hz. The coils were portable and had a sensitivity with the built in amplifier of about 500 mV/$\gamma$. Early attempts to detect the ULF waves at Arecibo and at Los Canos (7km away from the heater) did not produce any signals. These sites had large background noise levels due to household and industrial circuits. This prompted us to move the portable detectors to the uninhabited island of Mona, about 150 km west of the heater. The background noise at Mona was 6-10 db below the Puerto Rico stations. We report below the results of the experiments recorded at Mona.

Two types of experiments were performed. In the first one, the four HF transmitters were split in two pairs and the desired ULF frequency difference was introduced between each pair. The ULF frequencies generated were 3,5 and 6.25 Hz. This ULF frequency range was selected by the fact that they are nestled in a relatively low background region between the sub ULF geomagnetic fluctuations below 1-2 Hz

Nonlinear excitation of low frequency waves by the interaction of two high frequency (HF) waves or an amplitude modulated HF wave has, in addition to its intrinsic scientific interest, many practical applications. It has been suggested recently[1-5] that extremely efficient downconversion from HF to ULF can be achieved in the so called semicollisional regime, defined as the region where the frequency $\omega_3$ of the ULF wave is smaller than the electron-ion or electron neutral frequency $\nu$ (i.e. $\nu \gg \omega_3$). Two techniques were proposed in achieving this. The first relies on nonlinear coupling of two HF waves $(\omega_1, \underline{k}_1)$, $(\omega_2, k_2)$, satisfying the phase matching conditions

$$\begin{aligned} \omega_1 - \omega_2 &= \omega_3 \\ \underline{k}_1 - \underline{k}_2 &= \underline{k}_3 \end{aligned} \tag{1}$$

where $\underline{k}_3$ is the wavenumber of the ULF wave. The process has a power threshold decreasing [2,3] with $\omega_3$ and for $\omega_3 \ll \nu$ results in efficiency exceeding that expected on the basis of the Manley-Rowe relations. The second relies on the spontaneous magnetic field generation[4,5] by coupling the modulated hot spot temperature gradient ($\nabla T$) created by the HF heater to the ambient ionospheric density gradient ($\nabla n$). We report in this letter the first experimental verification of these nonlinear processes.

## ABSTRACT

We report the first experimental evidence for stimulated beat excitation of ULF waves by two HF pumps in the ionosphere, with conversion efficiency exceeding the one predicted by Manley Rowe relations. Both the low threshold for stimulated excitation and the high efficiency are consistent with theoretical predictions for helicon generation in the semicollisional regime, i.e. when the ion collision frequency is higher than the ULF frequency. Generation of ULF waves due to spontaneous generation of magnetic fields caused by the coupling of the heater induced temperature gradient to ionospheric gradient ($\nabla n \times \nabla T$) is also reported.

# ACTIVE NONLINEAR ULF GENERATION IN THE IONOSPHERE

S. Ganguly, W. Gordon

Department of Space & Astronomy

Rice University

Houston, Texas 77251

K. Papadopoulos*

Science Applications International Corporation

McLean, Virginia 22102

June 19, 1985

*Permanent Address: University of Maryland, College Park, Maryland 20742

## Appendix III

"Active Nonlinear ULF Generation in the Ionospehre"

S. Ganguly, W. Gordon and K. Papadopoulos

Sagdeev, R., and A. Galeev, *Nonlinear Plasma Theory*, Benjamin, New York, 1969.

Krall, N., and A. Trivelpiece, *Principals of Plasma Physics*, McGraw-Hill, New York, 1973.

Liu, C. S., Parametric instabilities in inhomoseneous unmagnetized plasma, *Adv. Plasma Phys.*, 6, 83, 1976.

Papadopoulos, K. and C. L. Chang, Generation of ELF/ULF waves in the ionosphere by dynamo processes, *Geophys. Res. Lett.*, *12*, 279, 1985.

Papadopoulos, K., K. Ko, and V. Tripathi, Parametric excitation of Alfven waves in the ionosphere, *J. Geophys. Res.*, *87*, 1491, 1982.

Papadopoulos, K., K. Ko, and V. Tripathi, Efficient parametric decay in dissipative media, *Phys. Rev. Lett.*, *51*, 463, 1983.

Perkins, F. W., and M. W. Goldman, Self-focusing of radio waves in a underdense ionosphere, *J. Geophys. Res.*, *86*, 600, 1981.

Reiman, A., Space-time evolution of nonlinear three-wave interactions, Ph.D. thesis, Princeton, Univ., Princeton, N. J., 1977.

Ferraro, A. J., H. S. Lee, R. Allshouse, K. Carrol, A. A. Tomko, F. J. Kelly, and J. R. Joiner, VLF/ELF radiation from the ionospheric dynamo current system modulated by HF signals, *J. Atmos. Terr. Phys.*, 44, 1113, 1982.

Germanstev, G. G., N. A. Zuikov, N. A. Mityakov, and Ya. Y. Eidleman, Combination frequencies in the interaction between high-power short-wave radiation and the ionospheric plasma, *JETP Lett*, Ensl. Transl., 20, 101, 1974.

Ginzburg, V. L., *The Propagation of Electromagnetic Waves in Plasmas*, Persamon, New York, 1970.

Gurevich, A. V., *Nonlinear Phenomena in the Ionosphere*, Sprinser-Verlas, New York, 1978.

Kapustin, I. N., P. A. Petrovskii, A. N. Yasil'ev, N. S. Smirnov, and O. M. Raspopov, Generation of radiation at combination frequencies in the resion of auroral electrojet, *JETP Lett*, Ensl. Transl., 24, 228, 1977.

Kaup, D., A. Reiman, and A. Bers, Space-time evolution of nonlinear three-wave interactions, I Internaction in a homoseneous medium, *Rev. Mod. Phys.*, 51, 275, 1979.

## REFERENCES


Ablowitz M. J., and H. Segur, *Solitons and the Inverse Scattering Transform*, Society for Industrial and Aplied Mathematics, Philadelphia, Pa. 1981.

Aisrain, P., in *Proc. Intern. Conf. on Semicond. Phys., Prague, 1960*, Academic, Orlando, Fla. 1961.

Berger, R., M. V. Goldman, and D. Dubois, Stiumlated diffusion scatterins in ionospheric modification, *Phys. Fluids, 18*, 207, 1975.

Bobroff, L., and H. Haus, Impulse response of active coupled wave systems, *J. Appl. Phys., 38*, 390, 1967.

Chans, C. L., V. Tripathi, K. Papadopoulos J. Fedder, P. J. Palmadesso, and S. l. Ossakow, Wireless seneration of ELF/VLF radiation in the ionsophere, in *Effect of the Ionosphere on Radiowave Systems*, edited by J. M. Goodman, p. 91, U. S. Government Printins Office, Washinston, D. C. 1981.

laser produced plasmas[4]. Namely the coupling of a density gradient $\nabla n$ with a hot plasma region produces a battery term proportional to $\nabla n \times \nabla T$, where T is the temperature of the hot region. This acts as a dynamo producing a magnetic field according to [4,5]

$$\frac{\partial B}{\partial t} = \frac{c}{en} (\nabla n \times \nabla T) \qquad (4)$$

As discussed in Ref. 5 the magnitude of the low frequency magnetic field produced by an oscillator temperature gradient is

$$B_3 = 100 \left[ \frac{Hz}{f_3} \right] \left[ \frac{\tilde{T}}{1000°k} \right] \left[ \frac{10km}{L_N} \right] \left[ \frac{10km}{L_T} \right] m\gamma$$

where $\tilde{T}$ is the oscillatory electron temperature due to the on-off HF heater operation, $L_N$ is the ionospheric density gradient and $L_T$ is the horizontal size of the hot spot. For our case $L_N \sim$ 50-60km, $L_T \sim$ 50km $f_3$ = 5Hz so that

$$B_3 = .8 \left[ \frac{\tilde{T}}{1000°k} \right] m\gamma$$

Namely $m\gamma$ fields can be achieved for oscillatory electron heating of the order of $\tilde{T} \sim 1000°k$. Such heating is not inconsistent with the one expected from the available HF power. Notice that Gordon and Carlson[7] observed F region electron temperature to increase by about 200°k when the HF power was about 4 to 5 times less than the present situation. As noted in Ref. 5 we believe that this process is the cause of the micropulsations at .01 and .02 Hz with amplitude of $5-10\gamma$ observed during on-off heating experiments by Stubbe and Kopka[8]. Before presenting our concluding remarks we should emphasize that both types of ULF generation presented here are different from the low frequency wave excitation by modulation of the polar or equatorial electrojet[6-10]. The latter is basically a linear process which requires the presence of ambient ionospheric currents. The modulated electron heating modulates the local ionospheric conductivity tensor. In the presence of d.c. currents, an a.c. current is generated by conductivity modulation which radiates at the modulation frequency.

In this letter we have presented: (i) The first experimental evidence for generation of ULF fields by stimulated beat excitation processes. The threshold power is consistent with the thresholds expected in the

semicollisional regime. An important finding for nonlinear physics is the verification of the prediction[2,3] that in this regime frequency downconversion efficiencies exceeding those predicted by Manley-Rowe can be achieved. (ii) Experimental verification for generation of ULF waves by spontaneous magnetic field generation due to the coupling of hot spot oscillatory temperature gradients with ambient ionospheric density gradients ($\nabla n \times \nabla T$). Further studies including scaling as well as more precise measurements are planned for the near future and will be reported elsewhere.

**ACKNOWLEDGMENT**

Arecibo Observatory is operated by Cornell University under a grant from N.S.F. We thank the Observatory personnel for their help and cooperation. We are grateful to H.F. Morrison and U. Conti of the University of Berkeley, Berkeley, California, for providing their equipment and expertise. J. Jost of GSFC, NASA and S.T. Noble of Rice University actively participated during the experiment. Thanks are due to C.W. Roberson for providing timely help during the staging of the campaign. Several discussions with Dr. A. Drobot are gratefully acknowledged. This work was supported in part by ONR N00014-77-C-1234 and ONR N00014-84-C-0353

## REFERENCES


1. K. Papadopoulos, R. Sharma and V. Tripathi, J. Geophys. Res. 87, 1491, 1982.
2. K. Papadopoulos, K. Ko and V. Tripathi, Phys. Rev. Lett. 51, 463, 1983.
3. K. Papadopoulos, K. Ko, A. Rieman and V. Tripathi in "Active Experiments in Space" ESA-SP 195, p. 11, 1983.
4. J.A. Stamper, K. Papadopoulos, R.N. Sudan, S.O. Dean, E.A. McLean and J.M. Dawson, Phys. Rev. Lett. 26, 1012, 1971.
5. K. Papadopoulos and C.L. Chang, Geophys. Res. Lett. 12, 279, 1985.
6. H.F. Morrison, W. Conti, V.F. Labson, E. Nichols, and N.E. Goldstein, Field Tests of Noise in SQUID and Induction Coil Magnetometers, University of California, Berkeley Report (April, 1984).
7. W.E. Gordon and H.F. Carlson, Radio Science 9, 1041, 1974.
8. P. Stubbe and H. Kopa, J. Geophys. Res. 86, 1606, 1981.
9. P. Stubbe, H. Kopka and R.L. Dowden, J. Geophys. Res. 9073, 1981.
10. A.J. Ferraro, H.S. Lee, R. Allshouse, K. Carrol, A.A. Tomko, F.J. Kelly and J.R. Joimer, VLF/ELF Radiation from the Ionosphere Dynamo Current Systems Modulated by HF Signals, J. Atmos. Terr. Physics, 44, 1113, 1982.

## FIGURE CAPTIONS

Fig. 1 Spectra of the received signal in the 0-10 Hz band. (February 14, 1985). Receiver was located at Mona Island. Data cover the period 1630 - 1830 AST. The HF transmitters were operating at 5.1 MHz and with a difference frequency $\Delta f$ of 5Hz during 1630-1730 AST, which was changed to 3Hz during 1730-1800 AST and changed back to 5.0 Hz during 1800-1830 AST. The magnitude of the 5.0Hz signals is about 160 $\mu rHz^{-\frac{1}{2}}$ and that of the 3.0Hz signal is about 340 $\mu VHz^{-\frac{1}{2}}$.

Fig. 2 Spectra for February 14, 1985, during 1737-1740 AST and 1821-1824 AST. The spectral bandwidth is 5 mHz. Note the large S/N ratios for both the 3 and 5 Hz signals.

Fig. 3 ULF signal generated when the HF was turned on/off at 100 m.s. rate. The receiver was located at Los Canos.

Fig. 4 Geometry of three-wave interaction in the ionosphere.

FEB 14, 1985; MONA ISLAND; E-W COMPONENT

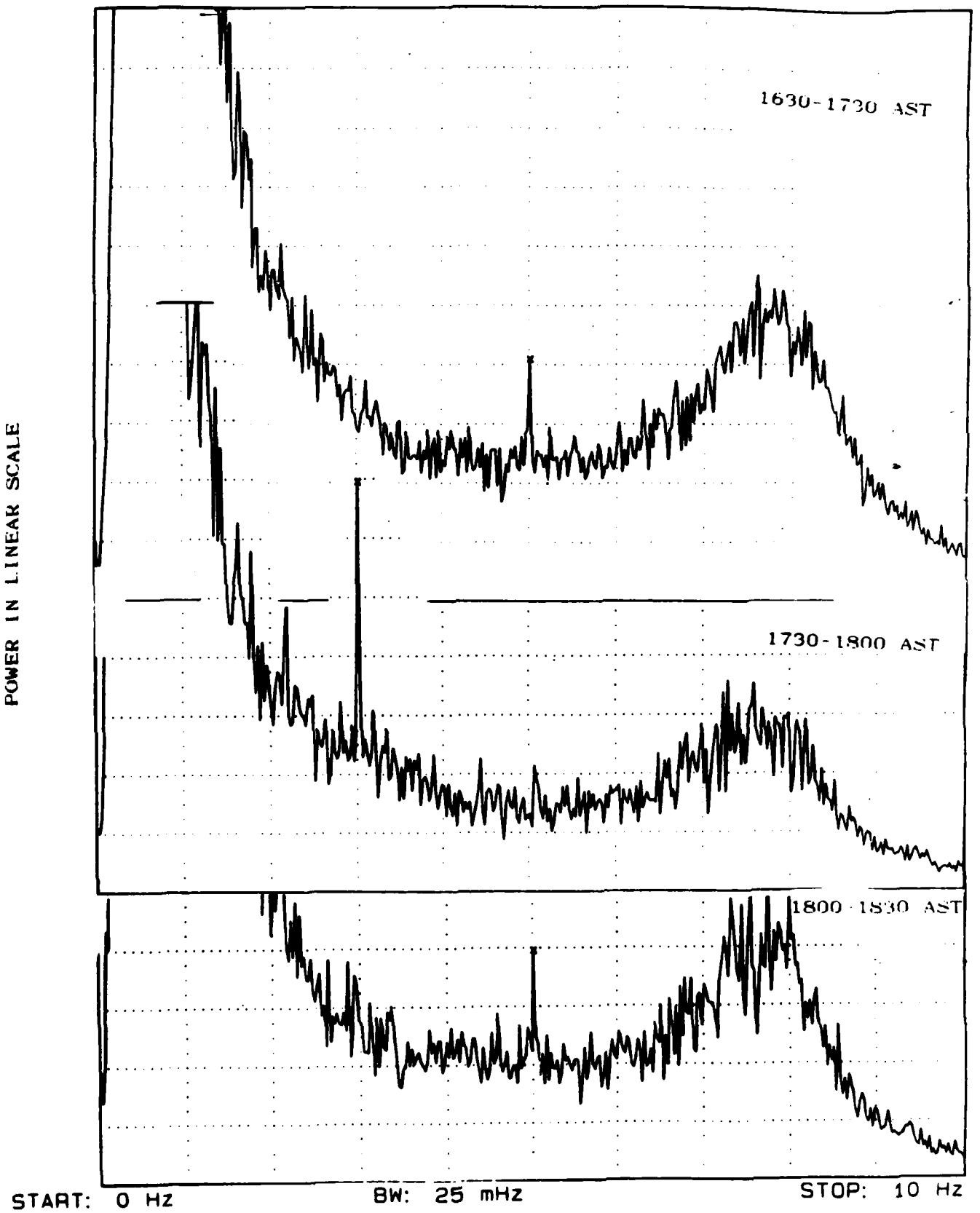

FEB 14, 1985; MONA ISLAND; E-W COMPONENT

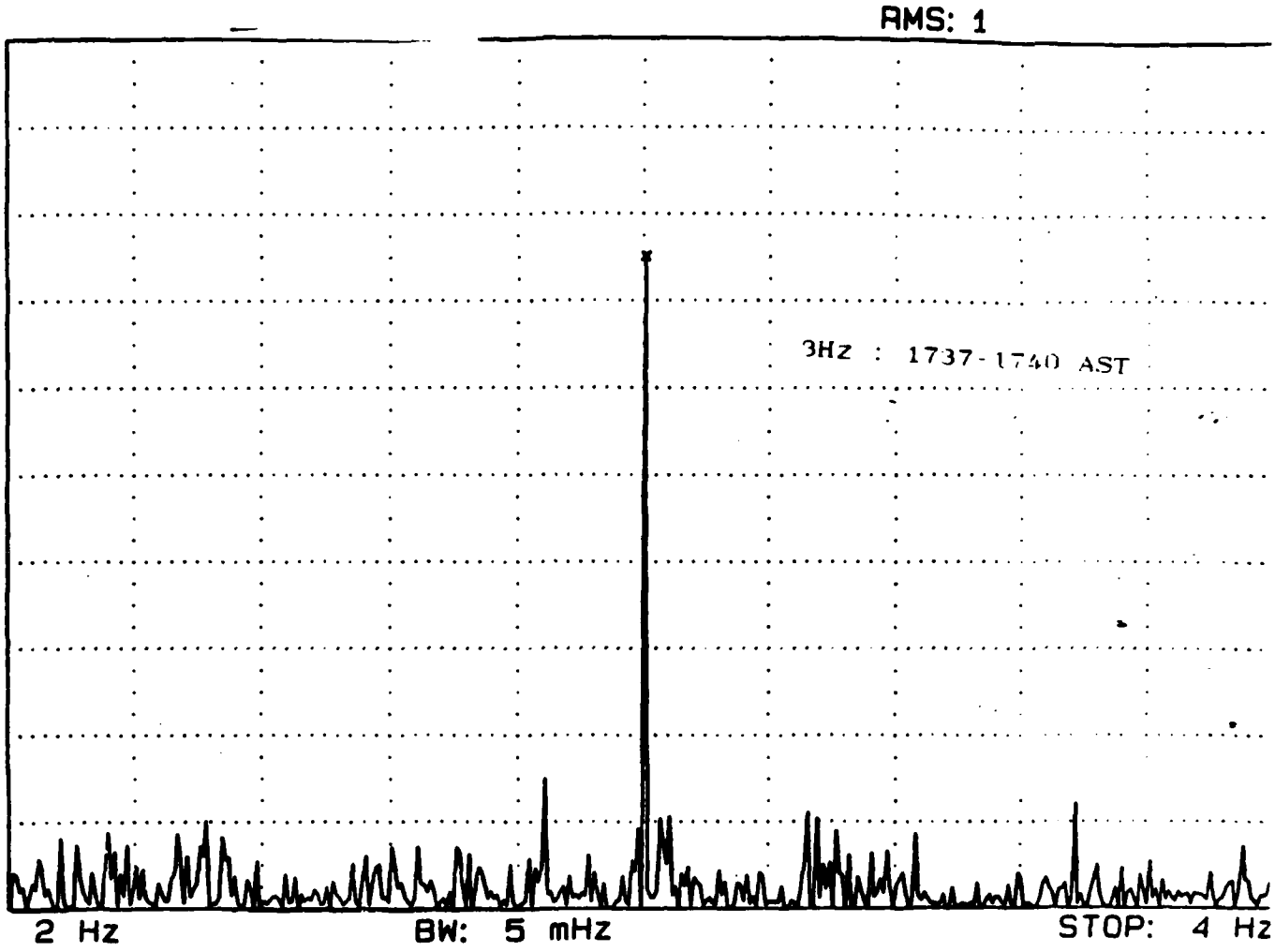


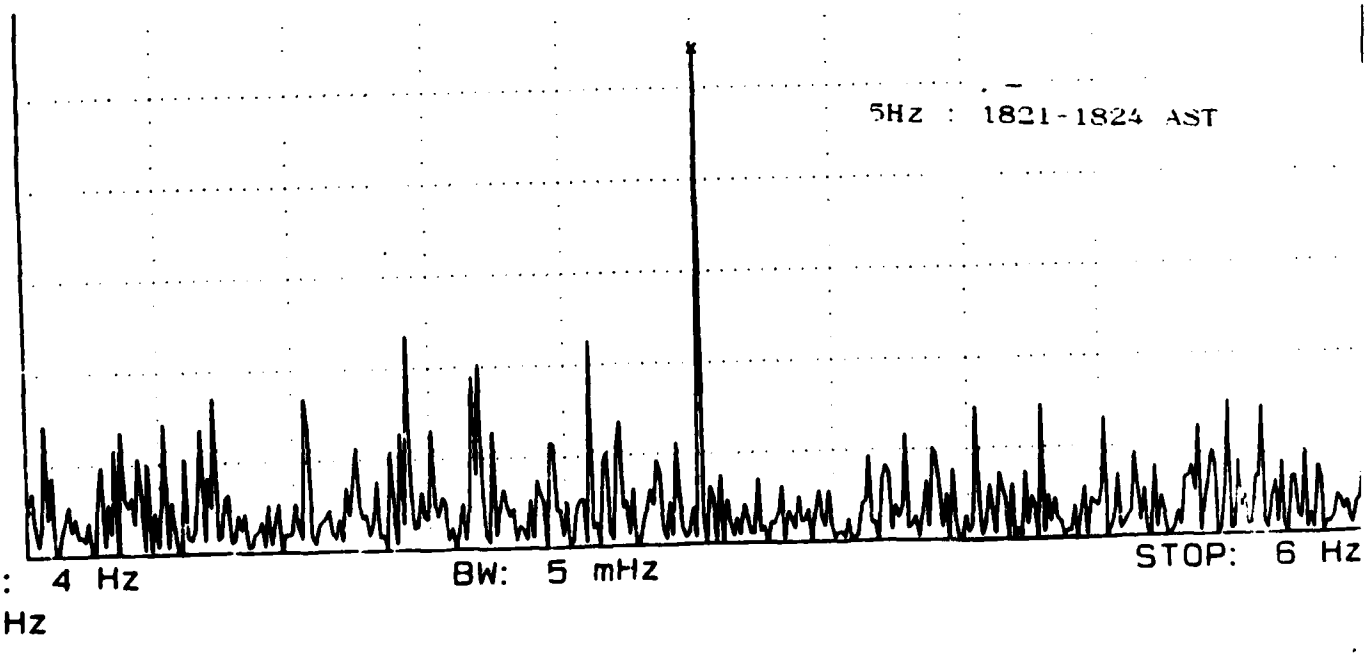

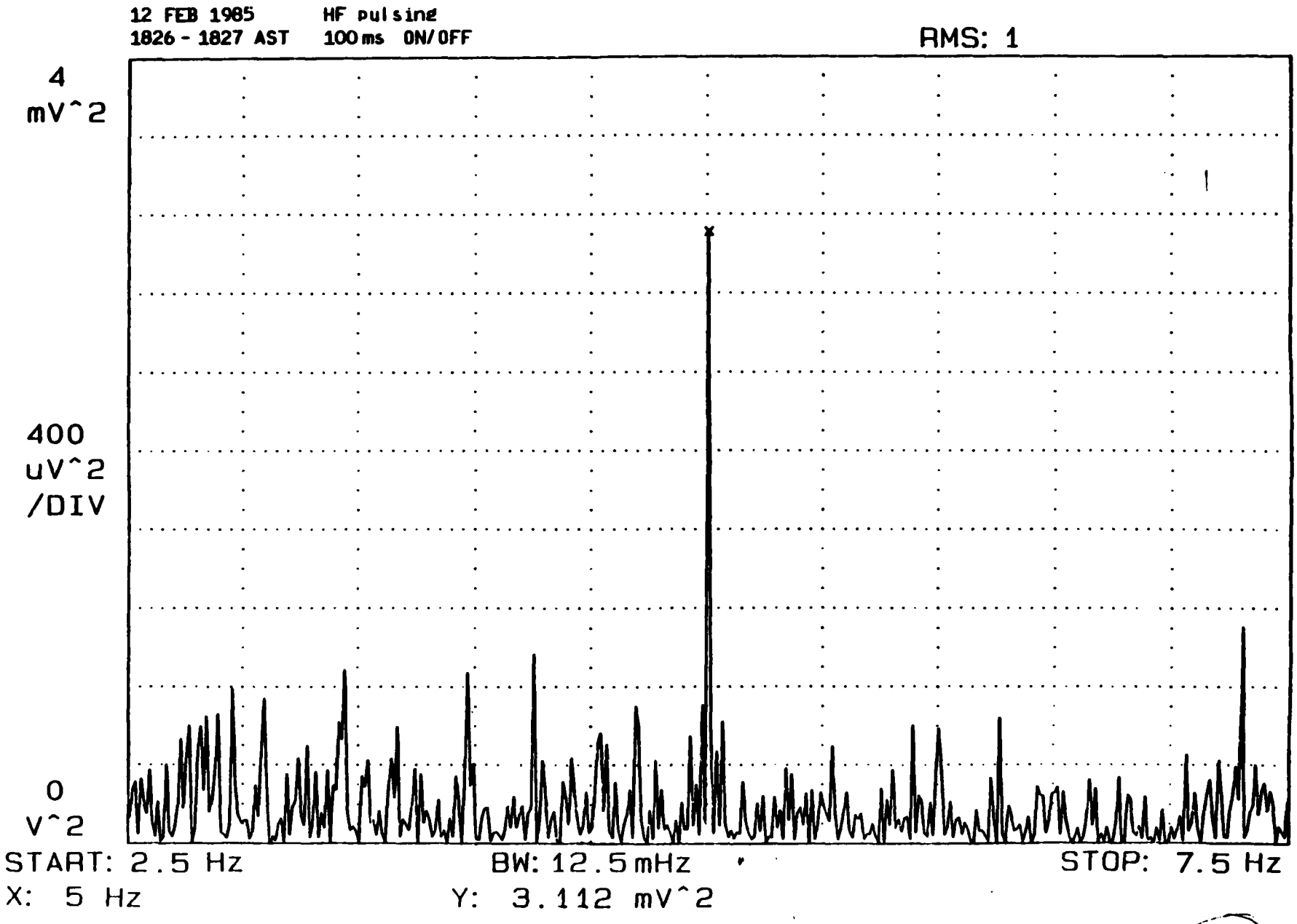
12 FEB 1985
1826 - 1827 AST
HF pulsing
100 ms ON/OFF
RMS: 1
4
mV^2
400
uV^2
/DIV
0
V^2
START: 2.5 Hz
BW: 12.5 mHz
STOP: 7.5 Hz
X: 5 Hz
Y: 3.112 mV^2

Fig 3

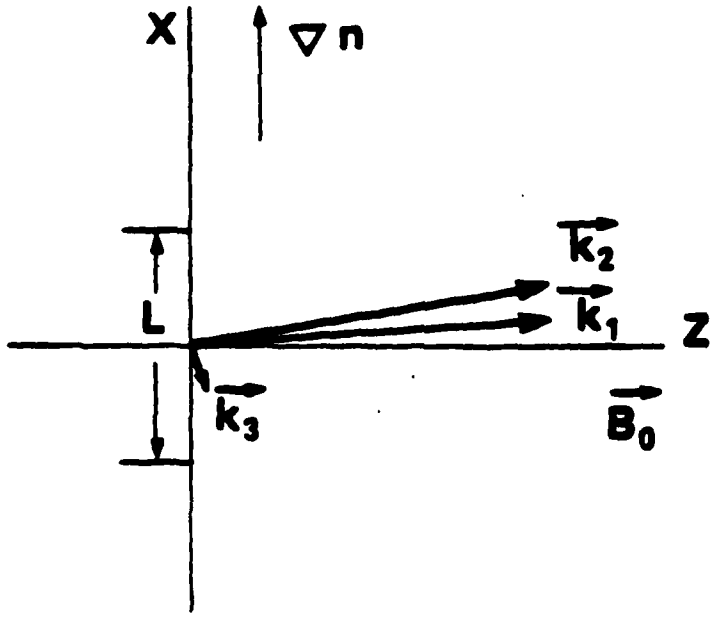


**FIGURE** 4

## Appendix IV

"Helicons in the Lower Ionosphere"

C.R. Menyuk and K. Papadopoulos

# HELICONS IN THE LOWER IONOSPHERE

by C.R. Menyuk and K. Papadopoulos

Helicons, waves which obey the dispersion relation

$$\omega = \frac{\Omega_e c^2}{\omega_e^2} k^2 \qquad (1)$$

where $\Omega_e$ is the electron cyclotron frequency and $\omega_e$ is the electron plasma frequency, have long been known to appear in solid-state plasmas for $\omega < \Omega_i$, all the way down to $\omega = 0$! This wave appears rather than the more familiar Alfvén wave because in solids the ions are frozen into place in the lattice, as a consequence of which, the plasma current is carried primarily by electrons, instead of by ions as is the case with the usual Alfvén wave.

In the D and lower E region of the ionosphere where $z < 110$ km, one finds that $\nu_i \gg \Omega_i$, i.e. the ion-neutral collision frequency is much greater than the ion cyclotron frequency.[2] It follows that the ions are viscously frozen and only electrons respond to the wave even when $\omega < \Omega_i$, so that helicons propagate in this region of the ionosphere, not Alfvén waves.

We begin by recalling the electron and ion equations of motion,

$$\underline{v}_e + \frac{ie}{m(\omega+i\nu_e)} \left[\underline{E} + \underline{v}_e \times \underline{B}_o/c\right] = 0,$$

$$\underline{v}_i - \frac{ie}{M(\omega+i\nu_i)} \left[\underline{E} + \underline{v}_i \times \underline{B}_o/c\right] = 0. \qquad (2)$$

Here, m and M are the electron and ion masses and e is the ion charge. (The ions, primarily $NO^+$ and $O_2^+$ in the lower ionosphere, are all singly-charged). The quantities $\nu_e$ and $\nu_i$ are the electron-neutral and ion-neutral collision frequencies. From this equation, we find

$$\underline{v}_e = \begin{bmatrix} \frac{ie}{m} \frac{(\omega+i\nu_e)}{[\Omega_e^2-(\omega+i\nu_e)^2]} & \frac{e}{m} \frac{\Omega_e}{[\Omega_e^2-(\omega+i\nu_e)^2]} \\ -\frac{e}{m} \frac{\Omega_e}{[\Omega_e^2-(\omega+i\nu_e)^2]} & \frac{ie}{m} \frac{(\omega+i\nu_e)}{[\Omega_e^2-(\omega+i\nu_e)^2]} \end{bmatrix} \underline{E}, \qquad (3)$$

$$\underline{v}_i = \begin{bmatrix} \frac{-ie}{M} \frac{(\omega+i\nu_i)}{[\Omega_i^2-(\omega+i\nu_i)^2]} & \frac{e}{M} \frac{\Omega_i}{[\Omega_i^2-(\omega+i\nu_i)^2]} \\ -\frac{e}{M} \frac{\Omega_i}{[\Omega_i^2-(\omega+i\nu_i)^2]} & -\frac{ie}{M} \frac{(\omega+i\nu_i)}{[\Omega_i^2-(\omega+i\nu_i)^2]} \end{bmatrix} \underline{E}$$

Writing $\underline{j} = n_o e(\underline{v}_i - \underline{v}_e)$, where $n_o$ is the ion density, and substituting into the field equation

$$k^2 \underline{E} = \frac{4\pi i\omega}{c^2} \underline{j} + \frac{\omega^2}{c^2} \underline{E} \quad , \tag{4}$$

where we are assuming for simplicity that the wave is propagating along the magnetic field lines, we now find

$$k^2 \underline{E} = \frac{\omega^2}{c^2} \begin{bmatrix} A & iB \\ -iB & A \end{bmatrix} \underline{E} \tag{5}$$

where

$$A = 1 + \frac{\omega_e^2(\omega+i\nu_e)/\omega}{[\Omega_e^2-(\omega+i\nu_e)]} + \frac{\omega_i^2(\omega+i\nu_i)/\omega}{[\Omega_i^2-(\omega+i\nu_i)]} \quad ,$$

$$B = -\frac{\omega_e^2\Omega_e/\omega}{[\Omega_e^2-(\omega+i\nu_e)]} + \frac{\omega_i^2\Omega_i/\omega}{[\Omega_i^2-(\omega+i\nu_i)]} \quad .$$

Equation (5) leads to the dipersion relation

$$k^2 = \frac{\omega^2}{c^2} \left[ 1 + \frac{\omega_e^2(\omega+i\nu_e)/\omega}{[\Omega_e^2-(\omega+i\nu_e)^2]} + \frac{\omega_i^2(\omega+i\nu_i)/\omega}{[\Omega_i^2-(\omega+i\nu_i)^2]} \right.$$

$$\left. \pm \frac{\omega_e^2\Omega_e/\omega}{[\Omega_e^2-(\omega+i\nu_e)^2]} \mp \frac{\omega_i^2\Omega_i/\omega}{[\Omega_i^2-(\omega+i\nu_i)]} \right] \quad . \tag{6}$$

We now reduce Eq.(6) using approximations appropriate for the region of the ionosphere which we are considering. To begin with,

$$\omega_e^2 - \Omega_e^2 \;\ll\; |\omega + i\nu_e|^2 \;\ll\; \Omega_i^2,\ \omega^2,\ \nu_i^2 \qquad , \quad (7)$$

from which we conclude

$$k^2 = \frac{\omega^2}{c^2}\left[\, 1 + \frac{\omega_i^2(\omega + i\nu_i)/\omega}{\Omega_i(\Omega_i \pm \omega \pm i\nu_i)} \,\right] \qquad , \quad (8)$$

where we have used the relation $\omega_e^2 / \Omega_e = \omega_i^2 / \Omega_i$. Dropping the displacement current contribution since we are interested in low frequency waves and using the relation

$$\nu_i \;\ll\; \Omega_i - \omega \ , \quad (9)$$

we conclude through first order in $\omega/\nu_i$ and $\Omega/\nu_i$,

$$k^2 = \pm \frac{\omega\,\omega_i^2}{\Omega_i c^2}\left[\, 1 \pm i\frac{\Omega_i}{\nu_i} \,\right] \qquad , \quad (10)$$

which leads to Eq.(1) if we neglect the small damping contribution.

AD-A159 359 ACTIVE IONOSPHERIC GENERATION OF ELF/VLF WAVES(U) 2/2
SCIENCE APPLICATIONS INTERNATIONAL CORP MCLEAN VA
K PAPADOPOULOS ET AL. 15 AUG 85 SAIC-85/1000
UNCLASSIFIED N00014-84-C-0353 F/G 4/1 NL

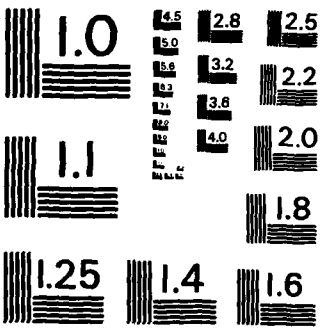


MICROCOPY RESOLUTION TEST CHART

NATIONAL BUREAU OF STANDARDS - 1963 - A

This mode appears ideally suited for ELF (extremely low frequency) communication applications[3,4] since the lower in the ionosphere one goes, the lower the wave attenuation becomes.

We thank Dr. K. Ko and Dr. A.T. Drobot for useful discussions. This work has been supported by O.N.R. contract # N00014-84-C-0353?

1. See S. Ichimaru, Basic Principles of Plasma Physics (W.A. Benjamin, Reading, MA, 1973). This mode was first discovered by O.v. Konstantinov and V.I. Perell, Zh.E.T.F. 38, 161 (1960) [Sov. Phys. J.E.T.P. 11, 117 (1960)] and by P. Aigrain in Proc. Int. Conf. on Semi-conductor Physics, Prague, 1960 (Academic, New York, 1961), p. 224. Dr. Aigrain later became Ministra de Science et Technologie in the cabinet of President Pompidou, which just goes to show how useful this mode can be!

2.?

3. K. Papadopoulos, K. Ko, and V. Tripathi, Phys. Rev. Lett. 51, 463 (1983).

4. K. Ko, C. Menyuk, A. Reiman, V. Tripathi, P. Palmadesso, and K. Papadopoulos (In Preparation).

END

FILMED

11-85

DTIC